



## UNIVERSITÀ DEGLI STUDI DI TORINO

This Accepted Author Manuscript (AAM) is copyrighted and published by Elsevier. It is posted here by agreement between Elsevier and the University of Turin. Changes resulting from the publishing process - such as editing, corrections, structural formatting, and other quality control mechanisms - may not be reflected in this version of the text. The definitive version of the text was subsequently published in *COMPUTERS AND GEOTECHNICS*, 54, 2013, 10.1016/j.compgeo.2013.05.010.

You may download, copy and otherwise use the AAM for non-commercial purposes provided that your license is limited by the following restrictions:

- (1) You may use this AAM for non-commercial purposes only under the terms of the CC-BY-NC-ND license.
- (2) The integrity of the work and identification of the author, copyright owner, and publisher must be preserved in any copy.
- (3) You must attribute this AAM in the following format: Creative Commons BY-NC-ND license (<http://creativecommons.org/licenses/by-nc-nd/4.0/deed.en>), 10.1016/j.compgeo.2013.05.010

The definitive version is available at:

<http://linkinghub.elsevier.com/retrieve/pii/S0266352X13000815>

1 **Debris flow hazard mitigation: a simplified**  
2 **analytical model for the design of flexible**  
3 **barriers**

4 Roberto Brighenti<sup>1</sup>, Andrea Segalini\*<sup>1</sup>, Anna Maria Ferrero<sup>2</sup>

5 <sup>1</sup>*Dept. of Civil-Environmental Engineering and Architecture, University of*  
6 *Parma, Viale G.P. Usberti 181/A - 43100 Parma – Italy, Ph. +39 0521 905910,*  
7 *Fax +39 0521 905924*

8 <sup>2</sup>*Dept. of Earth Science, University of Turin, Via Valperga Caluso 35 – 10135*  
9 *Torino – Italy, Ph. +39 011 6705114*

10 \* E-mail: [andrea.segalini@unipr.it](mailto:andrea.segalini@unipr.it)

11

12

13 **Abstract**

14 A channelized debris flow is usually represented by a mixture of solid particles of various sizes  
15 and water flowing along a laterally confined inclined channel-shaped region to an unconfined area  
16 where it slows down and spreads out into a flat-shaped mass.

17 The assessment of the mechanical behavior of protection structures upon impact with a flow, as  
18 well as the energy associated to it, are necessary for the proper design of such structures which, in  
19 densely populated areas, can prevent victims and limit the destructive effects of such a  
20 phenomenon.

21 In the present paper, a simplified analysis of the mechanics of the impact of a debris flow is  
22 considered in order to estimate the forces that develop on the main structural elements of a  
23 deformable retention barrier.

24 For this purpose, a simplified structural model of cable-like retention barriers has been developed -  
25 on basis of the equation of equilibrium of wires under large displacement conditions, - and the  
26 restraining forces, cable stresses and dissipated energies have been estimated.

27 The results obtained from parametric analyses and full-scale tests have then been analysed and  
28 compared with the proposed model.

29

30 **Keywords:** *Debris-flow, Barriers, Cable structure.*

31

32

33

34

1 **Nomenclature**

2  
3  
4

5	$A$	Cross section of a horizontal cable
6	$A_t$	Cross section of an equivalent cable representing the
7		transversal net
8	$d(t)$	Depth of a generic cable measured with respect to the
9		upper free surface of the accumulated material
10	$d_{ji}$	Relative vertical distance between cables $i$ and $j$
11	$e$	Horizontal distance between the first and the last edge
12		of a generic cable, measured normal to the cable
13	$E$	Young's modulus of the cable
14	$E_b, E_E$	Energy dissipated by the brakes and elastic energy
15		stored in the cables, respectively
16	$E_t$	Young's modulus of the equivalent transversal cables
17		representing the net
18	$f_b, f_{b,\max}$	Generic force and maximum allowable force in the
19		brake
20	$h(t)$	Height of the accumulated material at generic time $t$
21	$h_B$	Total height of the barrier
22	$h_0$	Constant height of the debris flow surge
23	$H$	Component along the x direction of the tension force
24		along a cable
25	$k, g$	Earth pressure and gravity acceleration coefficients
26	$L_i, l_i$	Effective length and projected length along the x-axes
27		of cable $i$ , respectively
28	$n$	Number of horizontal cables in the barrier
29	$p$	Constant vertical distance between the horizontal cables
30	$Q_i(x)$	Total horizontal load acting along a generic $i$ -th cable

1	$q_{c,j}, q_{ic}$	Horizontal load supported by cable $j$ due to load $q(z_i)$
2		acting on cable $i$ and the horizontal load supported by
3		cable $i$ when all the other cables are loaded by $q(z_j)$
4	$q_d(x)$	Horizontal load due to the dynamic pressure on the
5		barrier
6	$q_s(d, x)$	Horizontal load due to the static pressure on the barrier
7		at depth $d$
8	$q(z_i, t)$	Horizontal load, at time $t$ , acting directly on the cable
9		located at vertical co-ordinate $z_i$
10	$s_b, s_{b,max}$	Generic displacement and maximum allowable
11		displacement in the brake
12	$t$	Generic time instant
13	$r(z_j, z_i)$	Function defining the horizontal ratio between the
14		displacements of cable $i$ and cable $j$ (placed at vertical
15		coordinates $z_i$ and $z_j$ , respectively)
16	$T(x, d)$	Tension force along a cable (in a point having co-
17		ordinate $x$ ) placed at the depth $d$
18	$u(x)$	Horizontal displacement of a generic point, with co-
19		ordinate $x$ , of the cable (in the $y$ direction, as shown in
20		Figure 5)
21	$\bar{u} = u(x = l/2)$	maximum displacement of the cable, which occurs at its
22		midpoint
23	$V$	Components in the $y$ direction of the reaction forces
24		acting at the cable edges
25	$v_0$	Arrival velocity of the debris flow
26	$z$	Generic vertical co-ordinate of the horizontal cable
27	$z_i$	Generic vertical co-ordinate of the $i$ -th horizontal cable
28	$\alpha$	Empirical coefficient for dynamic pressure estimation
29	$\rho_d$	Mass density of the debris flow
30	$\theta$	Inclination angle of the slope
31	$Fr$	Flow rate of the debris [ $m^3/s$ ]

1	$\alpha$	Average inclination of the debris deposition behind the
2		barrier
3	$\mu$	Interface friction coefficient between landslide debris
4		and deposited debris
5	$T_f$	Duration of impact [s]
6		
7		

# 1. Introduction

Debris flows are rapid mass movements, composed of a mixture of grains, water and air, that develop under the effect of gravitational forces. The amount of energy involved in such phenomena is enormous and their mobility is such that it allows them to propagate for several hundreds of meters without losing their destructive potential. Owing to these characteristics, debris flows have been ascribed as being among the most dangerous and catastrophic of natural events [1]. The above cited phenomenon generally originates from collapses (landslides, erosions, etc.) associated with heavy precipitations due to extreme meteorological events such as heavy rainfall or rapid snowmelt. The characteristics that identify a debris flow are:

- A mixture of water and sediments (including sometimes vegetation debris);
- Unstable and non-uniform flow behaviour;
- High velocity of the mobilized mass and strong impact forces;
- Sudden phenomena of short duration.

Govi et al. [2] found, on the basis of a large number of observations that most of these phenomena generate in small to medium scale hydrological basins (up to 13 km<sup>2</sup>), around 40% of the observed phenomena develop along channels having a with a steeper slope than 35° and more than 40% of the occurrences have a recurring time of over 50 years. Several classification of these phenomena have been proposed by various authors (Pearson & Costa [3]; Costa [4]; Phillips & Davies [5]; Meunier [6]; Wan & Wang [7]; Coussot & Meunier [8]; Hungr et al. [9]; Takahashi [10]). The study of these phenomena is very difficult due to their short duration and unpredictability, the lack of historical data for a given basin and the complexity of the involved mechanical phenomena. Post event surveys allow some of the depositional features to be identified and provide indications on the maximum flow height. However, they lack information on the development of the phenomena with time. For this purpose, recursive events have been monitored out by several authors (Okuda et al. [11]; Marchi et al. [12]; Hürlimann et al. [13]; Tecca et al. [14]). Most of the studies, which had the aim of determining of the characteristic features of a debris flow, have been carried out in artificial channels, where the main involved variables were measured and others were controlled during the tests (Takahashi [10]; Iverson [15]). However, some uncertainties have

1 remained and other scaled models have been developed to simulate deposition  
2 mechanics (Mizumaya and Uehara [16]; Liu et al. [17]; Chau et al. [18];  
3 Deganutti et al. [19]; Ghilardi et al. [20]; Major [21]) but also to analyze  
4 transportation mechanics and energy dissipation [21]. Iverson [15] demonstrated  
5 that the uncertainties and difficulties in the interpretation of the experimental  
6 results are due to scale effects and to an incorrect artificial reproduction of natural  
7 phenomena.

8 In this work, a simplified structural model, developed by the Authors for the  
9 safety assessment of retention barriers against channelized debris flows, is  
10 presented and some parametric cases and a full scale test on debris flow barriers is  
11 interpreted through the proposed approach. This model has been developed as a  
12 simplified and efficient tool that can be used to verify of the supporting cables and  
13 foundations of a flexible debris flow barrier.

14 The present analytical and numerical-based approach has a different aim than that  
15 of a Finite Element Model (FEM). The numerical approach to the problem using  
16 3D FEM is in fact a well-known tool in this context (Ferrero [22]). However,  
17 computational experience using FEM modeling for these kinds of structures has  
18 shown that a large amount of time is needed for the geometrical setup of the  
19 model and several numerical instabilities develop due to the non linearity of the  
20 problem. The great effort required by FEM for this kind of problem limits the  
21 possibility of investigating different geometrical configurations, load schemes etc.  
22 It is in fact suitable to represent a specific configuration but does not allow  
23 investigation to be made of the influence of debris flow parameter modification  
24 (flow height and velocity, debris density etc.). On the other hand, parametrical  
25 analyses are common practice in geotechnical design because the aforementioned  
26 reasons. Consequently, the Authors decided to develop a simplified method  
27 (which is not yet available to our knowledge) that would allow several  
28 parametrical analysis to be performed in a limited time. Parametrical analysis  
29 should take into account the physical and mechanical features of debris flow  
30 which usually vary during debris development and which are consequently  
31 difficult to define in a deterministic way. It should be noted that no consideration  
32 has been given to the mechanical and physical behavior of debris flows in this  
33 paper. The proposed model involves the input parameters being acquired through  
34 a preliminary characterization of the design event. However, if the proposed tool

1 is adopted, the designer will be able to perform sensitivity analysis that will help  
2 to quantify the influence of parameter variability.

## 3 **2. Debris flow mechanics**

4 As already mentioned in the introduction, a detailed description of the complex  
5 mechanics of a debris flow is not the scope of this paper. This aspect has been  
6 studied by several authors considering the different phases that can be identified  
7 the debris flow development: the triggering phase [23], the run out phase (e.g.  
8 Hungr and Evans [24]; Pirulli [25], Takahashi [10]) and the deposition phase  
9 (Major [21], Vallance [26]). However, for the scope of this work, the most  
10 relevant aspect is the run out phase and, in particular, the determination of its  
11 velocity, volume and discharge rate, since debris flow impact power is connected  
12 to its kinetic energy, and to the energy dissipation effects during motion (Cesca  
13 [27]).

14 The velocity of a debris flow during its run out depends on several factors, such  
15 as: dip of the slope, the water mixture content, the grain distribution etc.. All these  
16 factors determine the relationship between the induced internal stresses and the  
17 deformation in relation to the applied external stresses, which is usually known as  
18 fluid rheology. Since the debris flow is a multi-phase mixture of different  
19 materials, its rheology somewhere falls in between the mechanical elastic  
20 behavior of the solid phase and the viscous behaviour of the liquid phase. All  
21 these aspects determine the kind of motion regime of the debris, which is mainly  
22 ruled by both inertia and viscosity forces. The well-known Bagnold number,  
23 determined in one of the pioneer works on debris flow rheology carried out by  
24 Bagnold [28], is the ratio between these two components (inertia and stresses due  
25 to viscosity) and can be used to identify different motion regimes. Bagnold used  
26 the term “macroviscous” to indicate a linear regime that is characterized by small  
27 Bagnold numbers, in which the shear stresses behave as in a Newtonian fluid with  
28 a corrected viscosity, and the term “grain-inertia” to indicate a regime that is  
29 characterized by large Bagnold numbers, in which the stresses are independent of  
30 the fluid viscosity but dependent on the square of the shear rate and on the square  
31 of the granular-phase concentration.

32 A rheological regime, usually termed “collisional”, which is based on the  
33 interaction between particles, during which momentum is exchanged and energy



1 is dissipated because of inelasticity and friction, has recently been defined  
2 (Goldhirsch [29], Jenkins and Hanes [30]; Hanes [31]).  
3 Armanini et al. [32] have shown how as both regimes can be simultaneously  
4 present in a debris flow: the behaviour can be reproduced by the kinetic theory in  
5 the proximity of the free surface, where the particle concentration is relatively  
6 small, while a layer dominated by frictional contacts can be observed near the  
7 static bed.

8 The study of debris flow strains and displacements is conveniently analysed  
9 considering three fundamental physical principles: mass, energy and momentum  
10 conservation, which lead to the driving equations. The above equations can be  
11 solved using several different methods: those based on continuum mechanics (i.e.  
12 the heterogeneous real mass is treated as a continuum) have been widely and  
13 successfully applied (e.g. Chen and Lee [33]; Denlinger and Iverson [34];  
14 McDougall and Hungr [35]).

15 When the debris thickness is far smaller than its extent (measured parallel to the  
16 bed), averaged depth Saint Venant equations can be used because the debris  
17 composition can reasonably be considered constant in a section, due to the limited  
18 height, thus avoiding the necessity of a complete 3-dimensional description of the  
19 flow (Savage and Hutter [36]).

20 The design of barriers against debris flows is based on the impact forces that are  
21 determined by the sum of the dynamic pressure (which can reach values up to the  
22 order of  $10 \text{ KN/m}^2$ ) and of the particle collision (which is characterized by values  
23 of  $100 \text{ KN/m}^2$  or more) (Suwa and Okuda [37]).

24 The dynamic impact can theoretically be estimated assuming an incompressible  
25 fluid hypothesis against a rigid barrier, and can be the assessed on the basis of  
26 momentum conservation for a steady fluid motion (Hungr [38]; Van Dine [39])  
27 while a theoretical solution for cable-like retention barriers is still not available.

## 28 **2.1 Forces induced by debris-barrier impact**

29 The pressure produced by the impact of a debris flow on the barrier can be  
30 estimated considering both the dynamic impact pressure and the static pressure of  
31 the deposited debris (Kwan & Cheung [40]). The former can be determined  
32 considering the well-known Bernoulli theorem; the kinetic energy of the flowing  
33 material,  $\rho_d \cdot v_0^2 / 2$ , is in fact into a pressure load when the velocity vanishes due

1 to the impact. The dynamic pressure on the barrier can thus be estimated as (Fig.  
2 1a):

$$q_d(x) = \alpha \cdot \rho_d \cdot v_0^2 \quad (1)$$

3 where  $\alpha$  is an empirical coefficient that varies between 1.5 and 5, according to  
4 Canelli et al. [41] and which can be assumed to be equal to 2.0 when the barrier is  
5 flexible and drained, the flow regime is granular and there is a lack of site  
6 specific information, where  $\rho_d, v_0$  are the density and the impact velocity of the  
7 debris, respectively. Studies have been carried out to back analyze some natural  
8 debris flow phenomena that have impacted monitored barriers [42] using a multi-  
9 stage surge model. However, some of the parameters involved in the analysis  
10 were estimated (i.e. the lateral earth pressure coefficient, the density of the debris,  
11 etc.) while others were measured directly (i.e. front velocity, surge height, etc.).  
12 An extensive analysis on design approaches for debris resisting barriers has been  
13 presented by Kwan & Cheung [40].

14 Generally, the debris could hit the barrier in the form of surges which fill the  
15 barrier either continuously or intermittently; the most critical impact scenario on  
16 barrier stability should always be chosen [40].

17 The thickness ( $h_0$ ) and velocity ( $v_0$ ) of moving debris surges can be estimated  
18 from debris mobility models using appropriate rheological parameters such as  
19 those recommended by Lo [43]. On the other hand, when the debris starts to  
20 accumulate behind the barrier, a static pressure can be assumed to occur (Fig. 1).  
21 The height of the accumulated material at the generic time  $t$  can be estimated, as  
22 shown in Eq. (2), by equating the volume of the material that arrives after such a  
23 time interval from the slope and the volume of the accumulated material behind  
24 the barrier (Fig. 1), (time  $t=0$  is assumed when the first particle of the debris-flow  
25 impacts the barrier) as:

$$h(t) = \sqrt{2 \cdot v_0 \cdot t \cdot h_0 \cdot \tan \theta} \quad (2)$$

26 In the above relation  $h_0, \theta$  are assumed to be the constant height of the debris  
27 flow surge and the inclination of the slope behind the barrier, respectively. It  
28 should be noted that, in order to use Eq. (2) it is necessary that  $\theta > 0$ . The static  
29 pressure acting at depth  $d(t)$ , measured with respect to the upper free surface of  
30 the material (Fig. 1b), can be assessed through the relation reported in Eq. (3), as

1 usually occurs in geotechnical science for the assessment of the static pressure  
 2 produced at a given depth:

$$q_s(d) = k \cdot d(t) \cdot \rho_d \cdot g = k \cdot \underbrace{(h_0 + h(t) - z)}_{d(t)} \cdot \rho_d \cdot g \quad (3)$$

3 where  $k, g$  are the earth pressure coefficient and the acceleration of gravity,  
 4 respectively, while  $z$  is the vertical position of the point under consideration (Fig.  
 5 1b).

6 By considering the barrier made up of  $n$  horizontal supporting cables -in the  
 7 following assumed to be placed at a constant relative distance of  
 8  $p = h_B / (n-1)$  for the sake of simplicity the pressure load  $q_i(z_i)$  (assumed to be  
 9 constant along each horizontal cable) acting on the  $i$ -th cable located at the  
 10 vertical co-ordinate  $z_i = h_B \cdot (i-1) / (n-1) \geq h_0$  can simply be calculated as in Eq.  
 11 (4) (the cables are numbered starting from 1 at the bottom of the barrier),

$$q(z_i \geq h_0, t) = \begin{cases} 0 & t < t_1 = (z_i - h_0)^2 / (2v_0 h_0 \operatorname{tg} \theta) \\ q_d = \alpha \cdot \rho_d \cdot v_0^2 & t_1 \leq t \leq t_2 = z_i^2 / (2v_0 h_0 \operatorname{tg} \theta) \\ q_s = k \cdot \left[ h_0 + h(t) - h_B \cdot \frac{(i-1)}{(n-1)} \right] \cdot \rho_d \cdot g & t > t_2 \end{cases} \quad (4)$$

12 while Eq. (5) should be used when the  $i$ -th cable is located at vertical coordinate  
 13  $z_i < h_0$

$$q(z_i < h_0, t) = \begin{cases} q_d = \alpha \cdot \rho_d \cdot v_0^2 & t < t_1 = z_i^2 / (2v_0 h_0 \operatorname{tg} \theta) \\ q_s = k \cdot \left[ h_0 + h(t) - h_B \cdot \frac{(i-1)}{(n-1)} \right] \cdot \rho_d \cdot g & t \geq t_1 \end{cases} \quad (5)$$

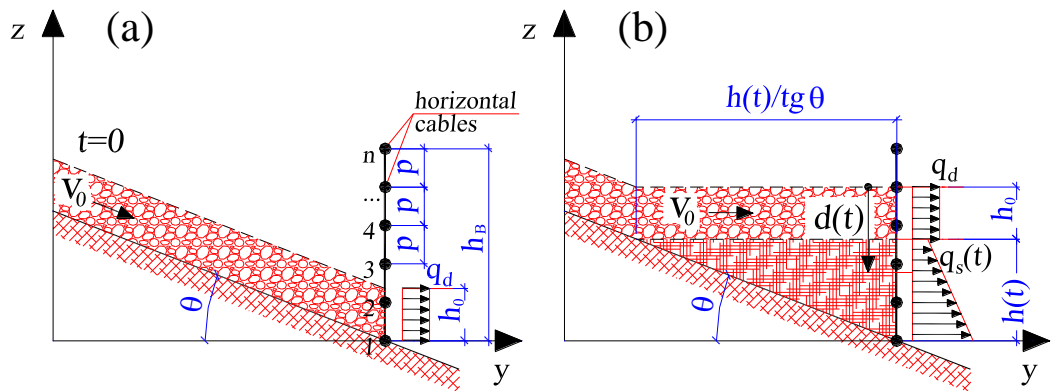
14 In others words, Eqs (4) and (5) enable one to evaluate the pressure exerted  
 15 directly on a given cable located at coordinate  $z_i$ , once its position with respect to  
 16 the flowing material and to the accumulated material is known. Eq. (4) is valid for  
 17 cables located at a greater height than the thickness of the flowing debris at  
 18 different time intervals: the cable is not yet in contact with the debris material for  
 19  $t < t_1 = (z_i - h_0)^2 / (2v_0 h_0 \operatorname{tg} \theta)$  and it is therefore unloaded; for the  
 20  $t_1 \leq t \leq t_2 = z_i^2 / (2v_0 h_0 \operatorname{tg} \theta)$  interval the  $i$ -th cable falls inside the portion of the  
 21 barrier that impacts with the flowing debris while the cable for  $t > t_2$  is in contact  
 22 with the material at rest behind the barriers. Similarly, Eq. (5) allows one to

1 estimate the pressure on a cable located at a coordinate  $z_i$  which is lower than the  
 2 thickness of the flowing material.  
 3 Since the cables are placed at a constant vertical distance of  $p$ , the distributed  
 4 load (assumed, for the sake of simplicity to act in a horizontal plane) acting on a  
 5 single cable of unit horizontal length is given by Eq. (6)

$$q_i(z_i, t) = q_i(d, t) = \begin{cases} p \cdot q(z_i, t) / 2 & i = 1, n \\ p \cdot q(z_i, t) & 2 \leq i \leq n-1 \end{cases} \quad (6)$$

6 The above and following relations are obviously not restricted by the hypothesis  
 7 of a constant  $p$ . More general relationships can be obtained for variable relative  
 8 cable distances. However, for the sake of analytical simplicity, such a hypothesis  
 9 has been introduced to illustrate the analytical model.

10 While calculating the pressure acting on the barrier, the model does not take into  
 11 account the deformation induced by the pressure exerted by the flowing granular  
 12 material; since the case of a rigid barrier is the most critical in the design of such  
 13 retention structures, the mitigation of the pressure, due to the barrier deformation,  
 14 can reasonably be neglected from the safety point of view. This hypothesis holds  
 15 true since the maximum transversal displacement of the barrier, as inferred from  
 16 both experimental and numerical results, is usually much lower (10 - 15%) than  
 17 the barrier extension (see Par. 4.2).



18

19 *Fig. 1. Debris accumulation behind the barrier and corresponding loads at a*  
 20 *generic time instant.*

21

22 The assumption of a constant load along the cable is an acceptable simplification  
 23 from the engineering safety point of view; this hypothesis allows one to treat the  
 24 problem as a two dimensional one, characterised by governing equations that can

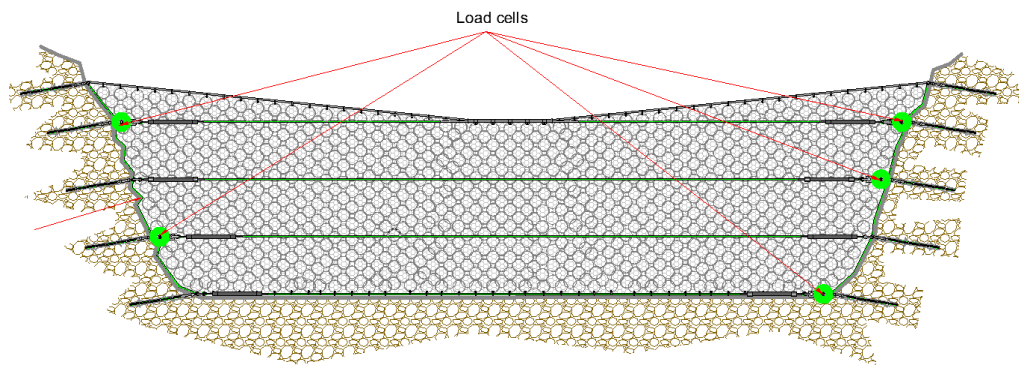
1 easily be handled for a simplified design of the retention barrier, as will be shown  
2 hereafter.

3

### 4 **3. Mechanics of cable-like retention barriers**

5 A simplified structural model for the assessment of the forces that develop in the  
6 retention barrier against a channelized debris flow can be formulated taking into  
7 account the typical structural lay-out of such elements.

8 The typical channelized debris flow barrier has an almost trapezoidal shape and is  
9 anchored to the ground (generally at the channel sides) by means of grouted  
10 anchors or cables. The main structural cables are horizontal and their number  
11 depends on the overall height and on the expected flow parameters (Fig. 2).



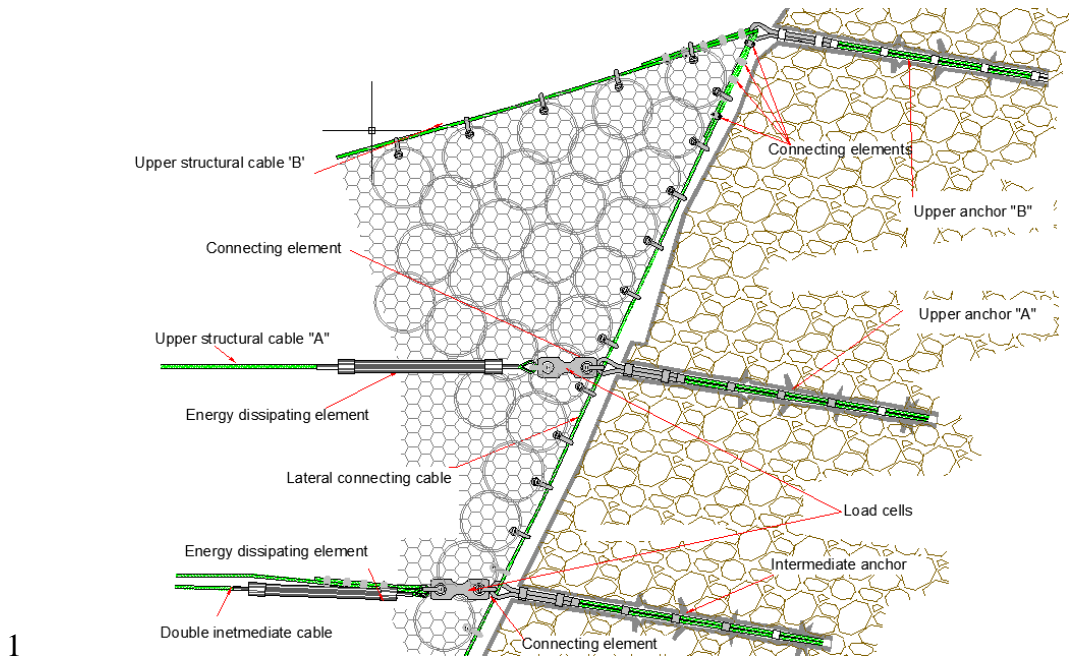
12

13 *Fig. 2. Typical structural lay-out of a net retention barrier against debris-flow.*  
14 *The single element features and the geometrical lay-out can vary according to the*  
15 *make and model of the barrier and to particular installation conditions (channel*  
16 *size, depth, etc.). The load cells referred to here are those that were used during*  
17 *on site tests carried out at the Pieve di Alpago (BL, Italy) test site (see Section 4 ).*

18

19 To each horizontal cable can be connected a dissipating element that would limit  
20 the amount of force transferred to its foundations during the debris flow impact  
21 (Fig. 3).

22 The structural net is typically formed by interconnected steel rings of  
23 homogeneous diameter (typically 30-50 cm); sometimes another net with smaller  
24 diameter openings is overlaid to the first one to retain smaller debris particles.



1  
2 *Fig. 3. Particular of the barrier foundations, dissipating elements and supporting*  
3 *cables. Single elements are variable with the make and model of the barriers*  
4 *available on the market.*



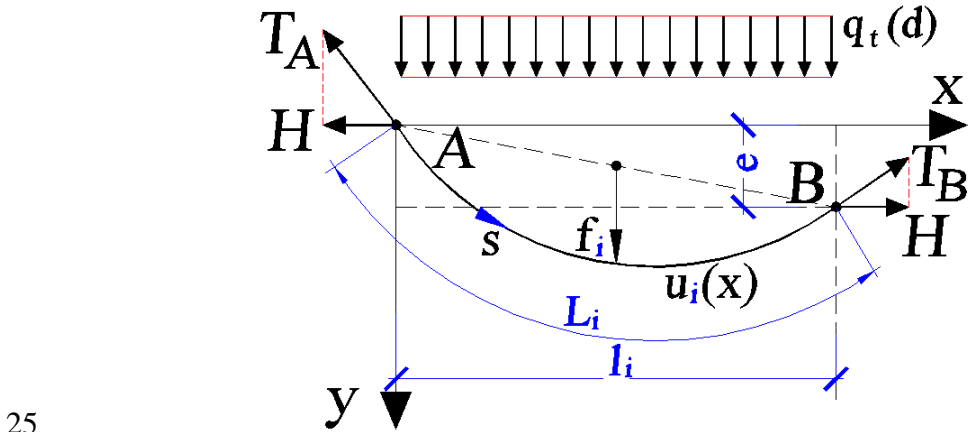
6  
7 *Fig. 4. Example of a debris flow barrier (installed at the Pieve di Alpago (BL,*  
8 *Italy) test site, see Section 4 ).*

9  
10 From the observation of Fig. 2 it can be noted that the main resisting elements are  
11 the horizontal cables fixed at their extremities to the foundations, while the net has

1 the role to retain the flowing solid particles and to transmit the developed forces to  
 2 the above described cables.  
 3 The governing equation of the equilibrium of a loaded cable can be usefully  
 4 employed to describe the mechanical behaviour of such a structural system.  
 5 Let us consider the barrier constituted by several horizontal cables mounted at a  
 6 reciprocal constant distance equal to  $p$ . The  $i$ -th cable - having its extremities  
 7 fixed at the points A and B - is characterized by a horizontal length equal to  $l_i$ ,  
 8 while its total effective length (when elongated under loading) is assumed to be  
 9 equal to  $L_i$  (Fig. 5). The distributed load acting on such a cable is assumed to lie  
 10 in an horizontal plane and to be constant with respect to the  $x$  co-ordinate at a  
 11 fixed time  $t$ . The load is, however, variable with time, since the depth  $d(t)$  of the  
 12 cable with respect to the top surface of the flowing material increases with  $t$  (Fig.  
 13 1b).  
 14

### 15 3.1. Formulation of the equilibrium equation of a cable-like structure

16 The present model, for sake of simplicity, considers the main resisting cables to  
 17 be loaded only in the horizontal direction by the forces produced by the debris  
 18 impact on the barrier, while the resultant of the vertical forces transmitted by the  
 19 connecting net to the single cable is considered as negligible. As a consequence,  
 20 only the deformation of the cables in the horizontal plane will be assumed to be  
 21 significant in the resistant mechanism of the structure.  
 22 Each cable of the barrier is assumed to have fixed extremities, i.e. the end points  
 23 of the cables are prevented to displace by some foundation system which  
 24 mechanical behavior is beyond the scope of the present research.



1 *Fig. 5. Scheme of the top view of a single cable under the forces produced by the*  
 2 *impact of a debris-flow, with related geometrical and static quantities.*

3

4 Starting from the equilibrium equation (Eq.(7)) of the  $i$ -th cable in differential  
 5 form at the time instant  $t$  [44],

$$\frac{d^2 u_i(t)}{dx^2} = -\frac{q(z_i, t)}{H_i} = -\frac{q_i(d, t)}{H_i} \quad (7)$$

6 after a double integration and by assuming a constant distributed load at a given  
 7 time instant  $q_i(d)$  (the dependence on time  $t$  for sake of brevity is not explicitly  
 8 indicated in the following relations) and the two extremities of the cable to be  
 9 located at the coordinates  $(x, y) = (0, 0)$  and  $(x, y) = (l_i, e)$  (referred to the  
 10 horizontal plane containing the cable, Fig. 5) corresponding to the points A and B,  
 11 respectively, the cable equation can be explicitly written as (Levy [45]):

$$u_i(x) = \frac{q_i(d)}{2H_i} (x \cdot l_i - x^2) + \frac{e}{l_i} x \quad (8)$$

12 where  $q_i(d) = q(z_i = h_b - d)$  is the constant horizontal load acting along the cable  
 13 under consideration placed at a depth  $d$  below the actual top free surface of the  
 14 flowing material, while  $H_i$  is the constant component along the  $x$  direction of the  
 15 tensile axial force  $T_i(x)$  in the cable [44]. Such a quantity can be obtained by  
 16 imposing the effective length of the cable to be equal to  $L_i$  through the equation:

$$L_i = \int_0^{l_i} \sqrt{1 + u_i'^2(x)} dx \quad (9)$$

17 which is obtained by integrating the trivial geometric relation

18  $dL_i = \sqrt{dx^2 + dy^2} = dx \sqrt{1 + u_i'^2(x)}$  (since  $dy = dx \cdot u_i'(x)$ ) that quantifies the  
 19 length of a generic curve which shape is described through the displacement  
 20 relation  $u_i(x)$ .

21 By denoting with  $f$  the quantity  $f = q_{ii} \cdot l_i^2 / 8H_i$  (see Fig. 5, where the  
 22 geometrical interpretation of  $f$  is represented, i.e. the maximum transversal  
 23 displacement measured with respect to the straight line A-B) and expanding in



1 Taylor series the expression of the integrand function in Eq. (9) (the dependence  
 2 on the depth  $d$  is omitted in the notation for simplicity), one can obtain:

$$L_i \cong l_i \cdot \left( 1 + \frac{8}{3} \frac{f^2}{l_i^2} + \frac{1}{2} \frac{e^2}{l_i^2} \right) + \dots \quad (10)$$

3 The sought term  $H_i$ , which can be demonstrated from equilibrium considerations  
 4 to be independent of  $x$ , can be finally obtained by using Eqs (8-10):

$$H_i \cong \frac{\sqrt{3}}{6} \cdot \frac{q_i \cdot l_i^2}{\sqrt{2L_i \cdot l_i - 2l_i^2}} \quad (11)$$

5 where the particular case characterised by  $e = 0$ , has been considered.

6 The tensile force  $T_i(x)$  acting along the cable can be also explicitly obtained  
 7 through the following relation (Levy [45]):

$$T_i(x) = H_i \cdot \frac{ds}{dx} = H_i \cdot \sqrt{1 + u_i'^2(x)} = H_i \cdot \sqrt{1 + \left[ \frac{q_i}{2H_i} (l_i - 2x) \right]^2} \quad (12)$$

8 by projecting the force  $H_i$  along the tangential direction of the cable in the point  
 9 of interest or, in other words, by calculating the product  $H_i \cdot ds/dx$ , where  $s$   
 10 denotes the curvilinear abscissa along the cable under consideration (Fig. 5).  
 11 At the two extremities of the cable, the components of the reaction forces in the  $y$   
 12 direction are given by the trivial value:

$$V_i(x=0) = V_i(x=l_i) = H_i \cdot \frac{du_i}{dx} \Big|_{x=0}^{x=l_i} = \frac{q_i \cdot l_i}{2} \quad (13)$$

13 The elastic deformation of the cables under loading must be also considered in  
 14 order to explicitly write the total effective length  $L_i$ ; in such a case the problem is  
 15 characterised by another source of nonlinearity due to the dependence of the cable  
 16 length  $L_i$  on the tensile force  $T_i(x)$  which depends itself on  $L_i$ .

17 Under limited deformation – 10-15% of the cable length - it can be assumed that  
 18 the tensile force  $T_i(x)$  is approximately equal to  $H_i$  (which does not depend on  $x$ )  
 19 all along the cable, i.e.  $T_i(x) \cong H_i = const.$  (since  $ds \cong dx$ ); in such a way the  
 20 effective length of the cable (assumed to obey the linear elastic Hooke's law)  $L_i$   
 21 can be written as:

$$L_i = l_i \cdot \left( 1 + \frac{H_i}{E_i A_i} \right) \quad (14)$$

1 The limited deformation of each cable is considered in order to maintain the  
2 appropriate functionality of the structure. According to Kwan & Cheung [40] the  
3 deformable barrier should sustain structural integrity for a deformation in the  
4 direction of the debris impact not lower than 10% of its total length and, in order  
5 to retain a considerable amount of material behind its deformed shape, it is  
6 suggested that the final deformation should not be greater than 15% of its total  
7 length.

8 The last relation used together with Eq. (11) allows to calculate – by solving the  
9 obtained non-linear problem – the effective cable length and the corresponding  
10 force  $H_i$  at the equilibrium state. The above assumption can be justified by  
11 considering that even for a cable having a noticeable transversal deformation  
12 such as  $f = 0.1 \cdot l_i$ , its effective length is  $L_i \cong 1.027 \cdot l_i$  (see Eq. (10)) and the axial  
13 force value along the cable lies in the range  $H_i \leq T_i(x) \leq 1.08 \cdot H_i$  (obtained by  
14 using Eqs (11) and (13)), while for  $f = 0.2 \cdot l_i$ ,  $L_i \cong 1.107 \cdot l_i$  and  
15  $H_i \leq T_i(x) \leq 1.28 \cdot H_i$ . It must be also recalled that, in debris flow net barriers, the  
16 presence of brakes is quite common; such a devices operate by dissipating energy  
17 and by increasing the cable length once the maximum allowable force of the brake  
18 is reached. Such an increased length produces a beneficial effect by inducing a  
19 decrease of the tension forces in the cables, while neglecting the brakes usually  
20 leads to a conservative design of the barriers. Such a topic will be discussed in  
21 Sect. 3.3 where the brakes modelling is presented.

22 The maximum displacement of the  $i$ -th cable occurring at its midpoint in the  
23 particular case  $e = 0$ , is equal to  $\bar{u}_i = u_i(x = l_i/2) = q_i \cdot l_i^2 / 8H_i$  (see Eq. (8)). The  
24 relation between the distributed load  $q_i$  and such a maximum displacement can  
25 thus be written from the solution of the equations below:

$$q_i(\bar{u}_i) = \frac{8H_i \cdot \bar{u}_i}{l_i^2} \quad (15)$$

$$\text{with } H_i \cong \frac{\sqrt{3}}{6} \cdot \frac{q_i \cdot l_i}{\sqrt{2} \sqrt{\left(1 + \frac{H_i}{E_i A_i}\right) - 1}} \rightarrow H_i = \left( \frac{q_i^2 \cdot l_i^2 \cdot E_i A_i}{24} \right)^{1/3}$$

1 where the relation for the approximate cable effective length evaluation (Eq. 14),  
 2 has been used together with Eq. (11); finally the sought relation  $q_i(\bar{u}_i)$  (see Eq.  
 3 (15<sub>1</sub>)) can be explicitly obtained:

$$q_i(\bar{u}_i) = \frac{64 E_i A_i}{3 l_i^4} \cdot \bar{u}_i^3 \quad (16)$$

4

### 5 **3.2. Effect of the net connections between cables**

6 Since the horizontal cables are connected by the barrier net, it can be assumed that  
 7 they are joined together by ‘equivalent’ vertical cables having the effect to  
 8 distribute a portion of the load directly applied to each horizontal cable to the  
 9 adjacent ones (Fig. 6a). The differential equilibrium equation Eq. (7) for the  $i$ -th  
 10 horizontal cable can thus be modified as:

$$\frac{d^2 u_i}{dx^2} = - \frac{q_i(x) - q_{ic}(x) + q_{ci}(x)}{H_i} = - \frac{Q_i(x)}{H_i} \quad (17)$$

11 in which  $q_{ic}(x), q_{ci}(x)$  represent the portion of the “direct” load  $q_i(x)$  acting on  
 12 cable  $i$  transferred to the adjacent cables and the “indirect” loads transmitted to the  
 13 cable  $i$  from the other loaded cables, respectively, i.e.:

$$q_{ic}(x) = \sum_{\substack{j=1 \\ j \neq i}}^n q_{i,j}(x), \quad q_{ci}(x) = \sum_{\substack{j=1 \\ j \neq i}}^n q_{j,i}(x) \quad (18)$$

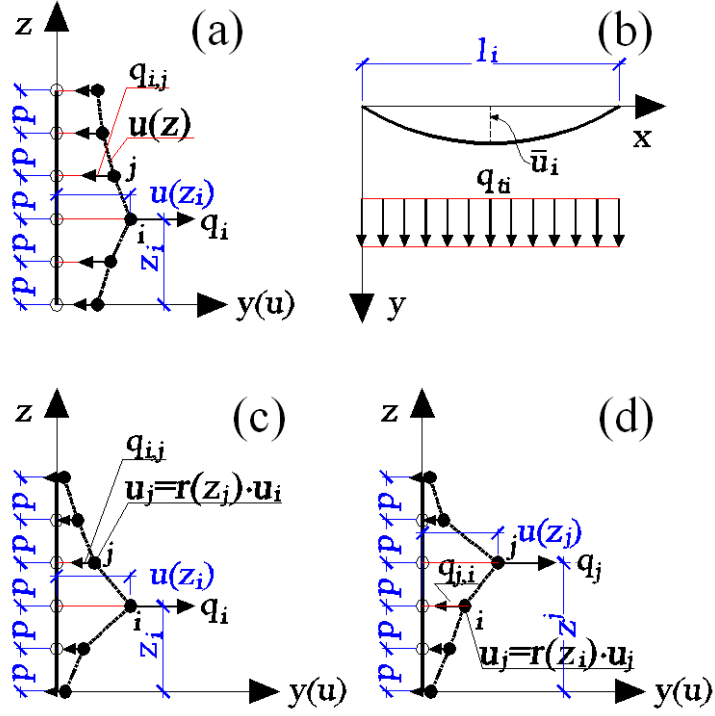
14 where  $q_{i,j}(x)$  is the “indirect” load carried by the cable  $j$  when the “direct” load  
 15  $q_i(x)$  is acting on the cable  $i$ , while  $q_{j,i}(x)$  is the “indirect” load carried by the  
 16 cable  $i$  when the “direct” load  $q_j(x)$  is acting on the cable  $j$ .

17 In other words, the load  $q_{ic}(x)$  represents the total fraction of the “direct” load  
 18 acting on the cable  $i$  carried by all the other cables  $j \neq i$ , while  $q_{ci}(x)$  represents  
 19 the sum of the portions of the “direct” loads acting on all the other cables  $j \neq i$   
 20 transferred to the cable  $i$ .

1 As previously stated, for sake of simplicity, it can be assumed the loads  
2  $q_i(x), q_{ic}(x)$  and  $q_{ci}(x)$  to be constant along the  $x$ -coordinate and acting on the  
3 horizontal plane containing each cable. The problem is now to estimate the loads  
4  $q_{i,j}$  and  $q_{j,i}$  in order to rewrite the equilibrium condition, given by Eq. (17), with  
5 the proper effective total transversal load  $(q_i - q_{ic} + q_{ci})$ . Due to the load-  
6 maximum deflection relationship given by Eq. (16), the loads  $q_{i,j}$  and  $q_{j,i}$  in Eq.  
7 (18) can be evaluated once the maximum displacement  $\bar{u}_{i,j}$  of the cable  $j$   
8 (produced by the distributed load  $q_i$  acting on cable  $i$ , Fig. 6a, c) or the maximum  
9 displacement  $\bar{u}_{j,i}$  of the cable  $i$  (produced by the load  $q_j$  acting on cable  $j$ , Fig.  
10 6d) are known.

11 It should be recalled that, in the real case, the cables in the barrier are not only  
12 subjected to horizontal loads but also to vertical ones due to the effect of the  
13 transversal net connecting them (see Figs 2-4). In a general case, by considering a  
14 distributed load acting on a single inclined plane along the whole cable, the  
15 deflection of a single wire takes place in a plane containing the cable extremities  
16 and the load direction, i.e. the present model can still be applied but in a different  
17 plane from the horizontal one.

18 It must be also considered as the vertical components of the forces acting along a  
19 single cable are significant only for the uppermost one, since the lower and the  
20 intermediate cables of the barrier are usually either restrained by the channel  
21 bottom or symmetrically surrounded by other cables, with the consequence of  
22 being subjected to a simple nearly horizontal force.



1

2 *Fig. 6. Scheme of the forces developed in cables  $j$  for a load acting on the cable  $i$*   
 3 *(a); horizontal cable under a concentrated load (b); simplified model for the*  
 4 *assessment of the load carried by the cables adjacent to cable  $i$  for a load  $q_i$*   
 5 *acting on it (c, d).*

6

7 By indicating with  $\bar{u}_{i,j}$  the maximum displacement occurring in cable  $j$  when the  
 8 cable  $i$  shows a maximum displacement equal to  $\bar{u}_i$ , an influence function  
 9  $0 \leq r(z_j, z_i) \leq 1$  (Fig. 6c, d) can be written in order to correlate the above  
 10 quantities as,

$$\bar{u}_{i,j} = r(z_j, z_i) \cdot \bar{u}_i \quad (19a)$$

11 the value of the distributed “indirect” load acting along the generic cable  $j$   
 12 transmitted from the cable  $i$  can be expressed as:

$$q_{i,j} = q_i \cdot \frac{r^3(z_j, z_i) \cdot C_j}{\sum_{k=1}^n r^3(z_k, z_i) \cdot C_k} \quad \text{with} \quad C_j = \frac{64 \cdot E_j A_j}{3l_j^4} \quad (19b)$$

13 The above relations can be obtained by writing the equilibrium condition for unit  
 14 cable length  $\sum_{j=1}^n q_{i,j} = q_i$ , and the  $n-1$  displacements relationships between the  
 15 cable  $i$  and the remaining cables  $j \neq i$ :

$$\bar{u}_i^{-3} = \left[ r(z_j, z_i) \cdot \bar{u}_j \right]^3 \quad \text{with} \quad j = 1, 2, 3, \dots, i-1, i+1, \dots, n \quad (20)$$

1 Eq. (20) correlates the value of the maximum displacement of the cable  $i$  with  
2 respect to the cable  $j$  by mean of the function  $r(z_j, z_i)$ . In other words, the above  
3 relations express the maximum deflection of the cable  $i$  by using the maximum  
4 deflection of the cable  $j$  multiplied by the influence function  $r(z_j, z_i)$ .  
5 Therefore, since there exists a direct relation between the distributed load acting  
6 on a cable and its maximum displacement (Eq. (16)), the load acting on a generic  
7 cable can be obtained once its maximum deflection is known.  
8 It can be observed that the function  $r(z, z_i)$  is representative of the mechanical  
9 properties of the vertical 'equivalent' cables connecting the horizontal ones: in  
10 fact, if the net connected to the horizontal cables is very weak, when the cable  $i$  is  
11 displaced by a certain amount the displacements in the other connected horizontal  
12 cables would result as depicted in Figs 6c, d, with a rapid decrease of the  
13 displacements values for an increasing vertical distance from the cable  $i$ . On the  
14 other hand, in the case of a strong connecting net, the displacements of the cables  
15 would be as depicted in Fig. 6a, with a lower reduction effect as the vertical  
16 distance from the displaced cable  $i$  increases.  
17 The governing equations (7) can be rewritten, using the above relations, as:

$$\frac{d^2 u_i}{dx^2} = - \frac{q_i - q_{ic} + q_{ci}}{H_i} = - \frac{q_i - \sum_{\substack{j=1 \\ j \neq i}}^n q_{i,j} + \sum_{\substack{j=1 \\ j \neq i}}^n q_{j,i}}{H_i} = \quad (21a)$$

$$= - \frac{\beta_i \cdot q_i \cdot \frac{r^3(z_i, z_i) \cdot C_i}{\sum_{k=1}^n r^3(z_k, z_i) \cdot C_k} + \sum_{\substack{j=1 \\ j \neq i}}^n \beta_j \cdot q_j \cdot \frac{r^3(z_j, z_i) \cdot C_i}{\sum_{k=1}^n r^3(z_k, z_j) \cdot C_k}}{H_i} = - \frac{Q_i}{H_i} \quad (21b)$$

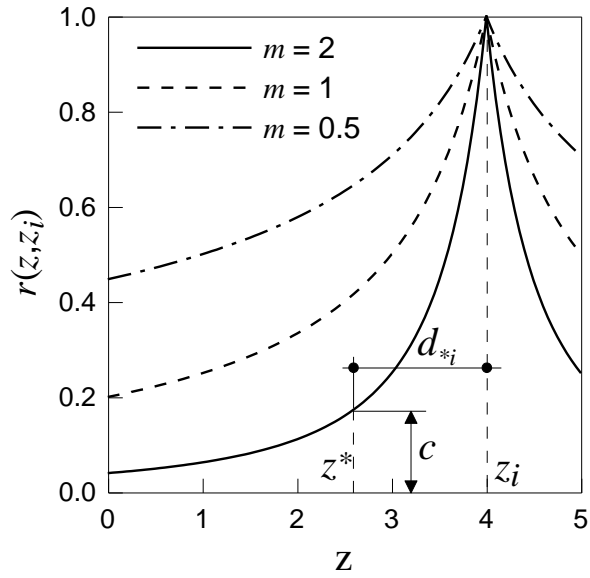
$$\text{with} \quad H_i = \left( \frac{Q_i^2 \cdot l_i^2 \cdot E_i A_i}{24} \right)$$

18 that represents a system of nonlinear second order ordinary differential equations  
19 with  $\bar{u}_j^{-3} = u_j^3(x = l_j/2)$ ,  $\bar{u}_i^{-3} = u_i^3(x = l_i/2)$  and the coefficient  $\beta_j = 1.0$  if  $q_j \neq 0$   
20 and  $\beta_j = 0$  if  $q_j = 0$ . The last cited coefficient needs to be introduced in order to

1 take into account for the possibility that not all the cables are loaded at the same  
 2 time.  
 3 It must be underlined as, in the above equations, any inertial effect is neglected  
 4 since the mass of the retention barrier is very small and the horizontal acceleration  
 5 of the cable and of the flowing material in contact with it can be supposed to be  
 6 low during the whole loading process.  
 7 The above introduced function  $r(z_j, z_i)$  can be reasonably assumed in the form:

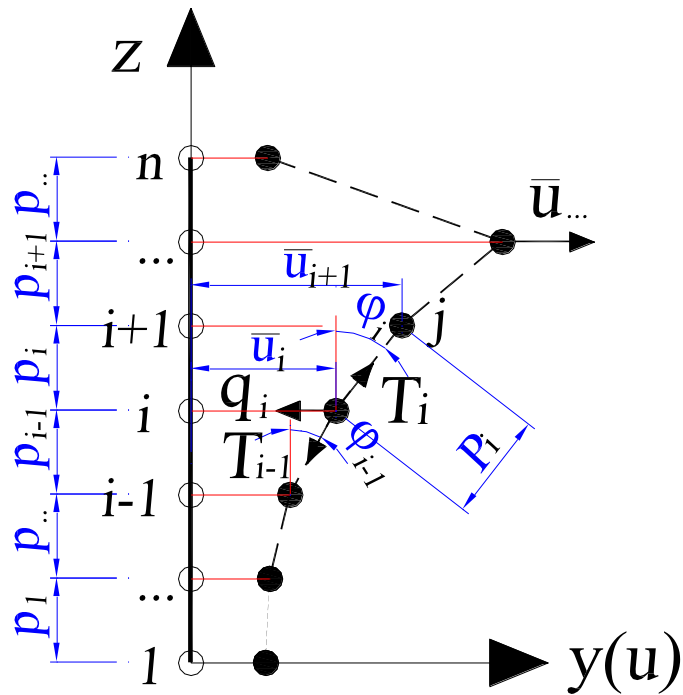
$$r(z_j, z_i) = \frac{1}{\left(|z_j - z_i| + 1\right)^{m_{ji}}} \quad \text{where} \quad m_{ji} = \frac{-\ln(c)}{\ln\left(|z^* - z_i| + 1\right)} \quad (22)$$

8 in which  $r(z^*, z_i) = c$  is the value attained by the function  $r(z_j, z_i)$  at the vertical  
 9 coordinate  $z_j = z^*$  (i.e. for a cable placed at a relative distance from cable  $i$  equal  
 10 to  $d^*_i = |z^* - z_i|$ ) while the unit value of  $r(z_j, z_i)$  is attained at  $z_j = z_i$  (Fig. 7).  
 11 The assumed  $r(z_j, z_i)$  indicates that the relation between the displacement of  
 12 different horizontal cables depends on their relative vertical distance  $d_{ji}$  and on  
 13 their reciprocal position. It can be observed that  $m_{ji} \neq m_{ij}$  due to the non-linear  
 14 force-displacement relationship (see Eqs (16) and (19b<sub>1</sub>)). This is due to the  
 15 difference between the relative displacement arising in cable  $i$  when cable  $j$  is  
 16 subjected to a given displacement, and the relative displacements arising in cable  $j$   
 17 when cable  $i$  is subjected to the same displacement.  
 18 The function  $r(z, z_i)$ , if properly tuned through its coefficient  $m_{ij}$ , can represent  
 19 the relation between the displacements of two connected cables.  
 20



1  
2  
3  
4

Fig. 7. Assumed pattern of the function  $r(z_j, z_i)$  for different values of the exponent  $m$  and for  $z_i = 4$  in Eq. (22).



5  
6  
7  
8

Fig. 8. Scheme of a vertical section of the barrier; the horizontal cables are represented by filled circles.

9 The determination of the function  $r(z, z_i)$  can be achieved by considering the  
10 mechanical behaviour of the transversal midsection of the barrier (Fig. 8). The



1 equilibrium condition in the horizontal direction for the  $i$ -th cable can be written  
 2 as:

$$q_i = T_i \sin \varphi_i - T_{i-1} \sin \varphi_{i-1} \quad (23)$$

$$\text{with } \sin \varphi_i = \frac{\bar{u}_i - \bar{u}_{i-1}}{P_i}, \text{ and } P_i = \sqrt{p_i^2 + (\bar{u}_i - \bar{u}_{i-1})^2},$$

$$T_i = A_{ii} \cdot E_{ii} \cdot \varepsilon_i = A_{ii} \cdot E_{ii} \cdot \frac{\overbrace{P_i - p_i}^{\varepsilon_i}}{P_i} = A_{ii} \cdot E_{ii} \cdot \frac{\sqrt{p_i^2 + (\bar{u}_i - \bar{u}_{i-1})^2} - p_i}{P_i}$$

3 where  $\varepsilon_i$  is the strain in the vertical cable connected to the horizontal cable  $i$ .

4 On the other hand the relation between the applied load and the maximum

5 transversal deflection of the cable is given by  $q_i = (64 \cdot E_i A_i / 3l_i^4) \cdot \bar{u}_i^3$  (see

6 Eq.(16)). The above equilibrium equations (23) can thus be rewritten as:

$$q_i = \frac{64 E_i A_i}{3l_i^4} \cdot \bar{u}_i^3 = T_i \sin \varphi_i - T_{i-1} \sin \varphi_{i-1} = A_{ii} E_{ii} \cdot \frac{\sqrt{p_i^2 + (\bar{u}_i - \bar{u}_{i-1})^2} - p_i}{P_i} \cdot \frac{\bar{u}_i - \bar{u}_{i-1}}{P_i} - A_{i-1} E_{i-1} \cdot \frac{\sqrt{p_{i-1}^2 + (\bar{u}_{i-1} - \bar{u}_{i-2})^2} - p_{i-1}}{P_{i-1}} \cdot \frac{\bar{u}_{i-1} - \bar{u}_{i-2}}{P_{i-1}} \quad (24)$$

7 Eq. (24) simply states the equilibrium of the load acting on the cable under study  
 8 and those deriving from the other connected cables, expressed by means of their  
 9 maximum horizontal displacements.

10 Once the maximum transversal deflection  $\bar{u}_k$  of the  $k$ -th cable is known, the  
 11 maximum transversal deflections of the other cables can be obtained by the  
 12 solution of the system of nonlinear equations ( see Eq. (24)).

13 The solution of such a system is very awkward and does not allow an easy  
 14 analytical treatment to get sought values. For such a reason the determination of  
 15 the solution can be obtained through a numerical method; in the present paper an  
 16 iterative evolutionary algorithm belonging to the Genetic Algorithm (GA)  
 17 approaches is applied (Goldberg [46]; Gen and Cheng [47]).

18 In many physical problems, the solution of their mathematical formulation is often  
 19 quite difficult to be determined by applying classical approaches. An increasing  
 20 interest in a class of algorithms known as Genetic Algorithms (GAs), which  
 21 operate by simulating the natural evolutionary processes of life - the Darwinian  
 22 survival of the fittest principle is applied by iteratively improving the current

1 solution [46], [47], has been observed during last decades. Such algorithms  
 2 represent random stochastic methods of global optimisation, and are used to  
 3 minimise or maximise a chosen objective function suitable for a given problem.  
 4 Genetic algorithms have successfully been applied to analyse several problems  
 5 such as structural performance optimisation (Gantovnik et al. [48]; Brighenti [49];  
 6 Brighenti et al. [50]) and material design and parameters identification (Zohdi  
 7 [51]) as well as several non-structural problems.  
 8 By using the above cited biological-based algorithm approach, the fulfilment of  
 9 some conditions related to a desired objective function can be approximately  
 10 imposed; in the present case the objective function to be minimised can be  
 11 assumed to be represented by the total error  $e_{tot}$  in satisfying the equilibrium  
 12 equations of the system (24), i.e.:  $e_{tot} = \min$

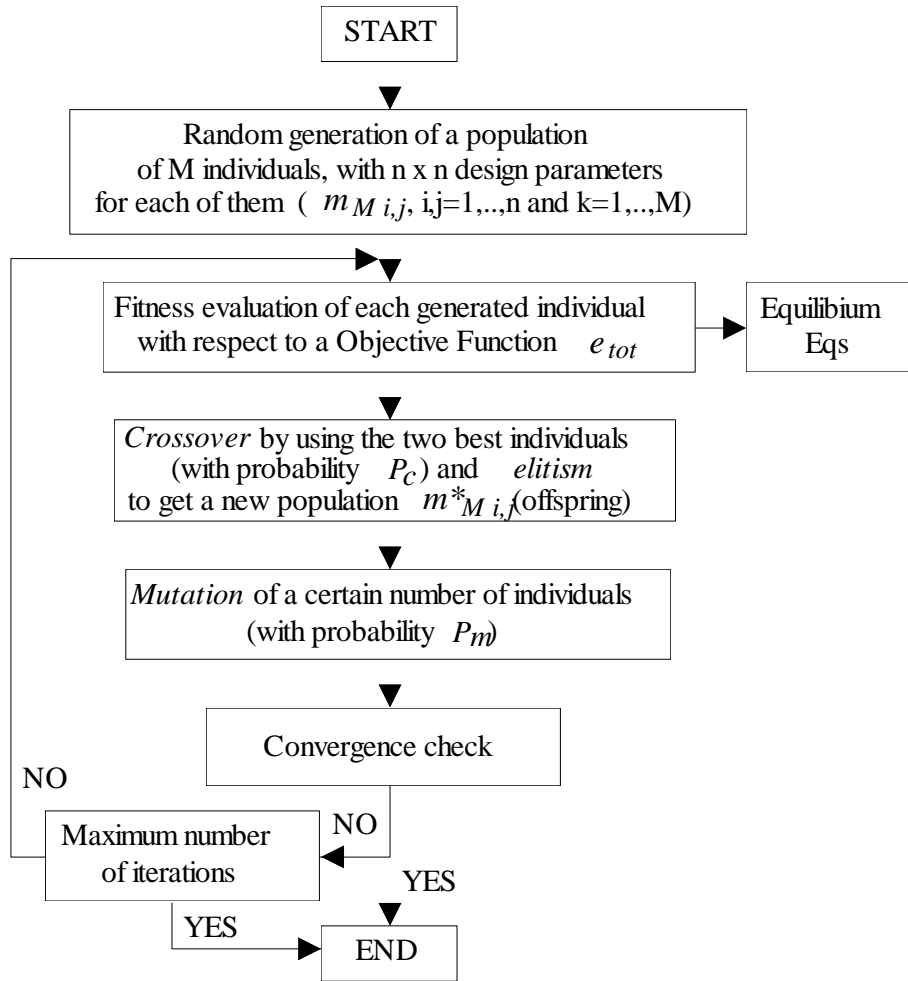
$$e_{tot} = \sum_{i=1}^n |e_i| \quad \text{with} \quad (25)$$

$$e_i = \frac{64E_i A_i}{3l_i^4} \cdot \bar{u}_i^3 - A_i E_i \cdot \frac{\sqrt{p_i^2 + (\bar{u}_i - \bar{u}_{i-1})^2} - p_i}{p_i} \cdot \frac{\bar{u}_i - \bar{u}_{i-1}}{P_i} +$$

$$+ A_{i-1} E_{i-1} \cdot \frac{\sqrt{p_{i-1}^2 + (\bar{u}_{i-1} - \bar{u}_{i-2})^2} - p_{i-1}}{p_{i-1}} \cdot \frac{\bar{u}_{i-1} - \bar{u}_{i-2}}{P_{i-1}}$$

13 In Fig. 9 the flow-chart of the developed Genetic Algorithm used to minimize the  
 14 errors expressed by Eq. (25) is reported. As can be observed, several initial  
 15 random generations of the sought solution represented by the exponents  $m_{ij}$  are  
 16 required (initial population made of  $M$  individuals). Performing the fitness  
 17 evaluation of each individual (quantified through the violation of the equilibrium  
 18 equations measured by  $e_{tot}$ ), the highest ranking results can be identified and used  
 19 for subsequent crossover and mutation operations to be carried out in order to get  
 20 a new offspring of new individuals to be treated again as the previous one  
 21 (Brighenti [49]; Brighenti et al. [50]). By repeating the above process, in an  
 22 iterative way, up to the fulfillment of a given error tolerance, the numerical  
 23 solution tends to the true solution of the problem.

24  
 25



1

2

Fig. 9. Flow chart of the Genetic Algorithm used for the solution of the system given by Eqs (25).

3

4

5

As an example, the solution obtained by the GA in the case of 11 equally spaced cables having the same mechanical properties (cross section area, Young modulus and equal length) in which the sixth cable is displaced by a unit quantity ( $\bar{u}_5 = 1$ ) is shown in Fig. 10.

9

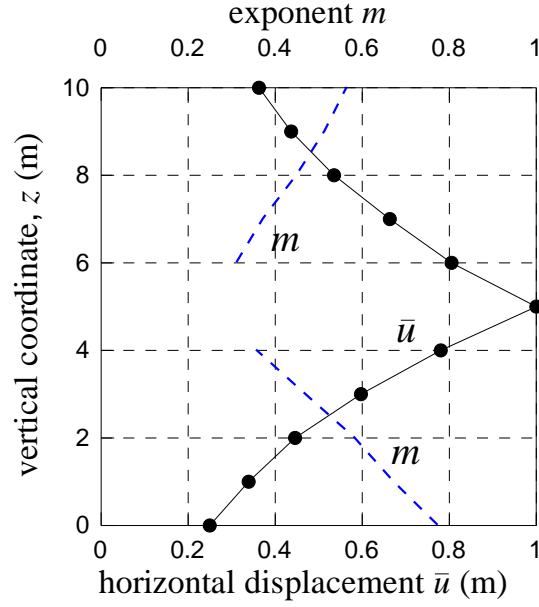
10

It can be observed as the deformed pattern, obtained through the GA approach, is reasonably correct and that the corresponding exponent  $m_{j5}$  of the  $r(z_j, z_5)$  law, evaluated for each couple of cables by considering the sixth cable as the reference one, is variable in the range 0.3-0.8 (see dashed line in Fig. 10).

11

12

13



1

2 *Fig. 10. Deformed pattern of 10 horizontal identical cables, joined by vertical*  
 3 *cables, obtained through the GA; the corresponding exponent  $m$  of the  $r(z_j, z_5)$*   
 4 *law (Eq. (22)) is also reported (dashed line).*

5

6 It can be observed as the particular case of totally independent cables can be  
 7 simulated by assuming  $m_{ji} \rightarrow \infty$  in the expression of  $r(z_j, z_i)$  (Eq. (22)); in such  
 8 a particular case the differential equations become uncoupled and can be written  
 9 as:

$$\frac{d^2 u_i}{dx^2} = -\frac{q_i}{H_i} \quad i = 1, 2, \dots, n, \quad (26)$$

with boundary conditions  $u_i(0) = u_i(l_i) = 0$  and  $L_i = \int_0^{l_i} \sqrt{1 + u_i'^2(x)} dx$

10

11 Finally, since the solutions of the equilibrium equations given by Eq. (8) can be  
 12 observed to be characterised by the same patterns scaled by the value of the  
 13 applied uniform load, the above Eqs (21) can be written by considering only the  
 14 central maximum displacement for each cable, i.e.

$$\bar{u}_i = u_i(l_i/2) = \frac{\beta_i \cdot q_i \cdot \frac{r^3(z_i, z_i) \cdot C_i}{\sum_{k=1}^n r^3(z_k, z_i) \cdot C_k} + \sum_{\substack{j=1 \\ j \neq i}}^n \beta_j \cdot q_j \cdot \frac{r^3(z_j, z_i) \cdot C_i}{\sum_{k=1}^n r^3(z_k, z_j) \cdot C_k}}{2H_i} \cdot \frac{l^2}{4} = \frac{Q_i \cdot l_i^2}{8H_i} \quad (27)$$

1 In other words, the system of cables is assumed to be governed by  $n$  independent  
2 variables,  $\bar{u}_i$ , that is to say that every cable is completely described by one single  
3 parameter (degree of freedom) corresponding to its central and maximum  
4 horizontal displacement  $\bar{u}_i$ .  
5 As a representative example, at the generic time instant  $t$  at which we assume to  
6 have  $q_{t1}(t) \neq 0$ ,  $q_{t2}(t) \neq 0$ ,  $q_{t3}(t) \neq 0$ , while  $q_{t4}(t) = q_{t5}(t) = \dots = q_{tm}(t) = 0$ , in the  
7 case of cables having equal length  $l$ , cross section area  $A$  and elastic modulus  
8  $E$ , the system of governing nonlinear equations becomes:

$$\left\{ \begin{array}{l} \frac{8}{l^2} \bar{u}_1 = \frac{q_1}{H_1} \sum_{\substack{j=1 \\ j \neq 1}}^3 \frac{C_1^3 r^3(z_1, z_j)}{D_1} + \frac{C_1}{H_1} \sum_{\substack{j=1 \\ j \neq 1}}^3 \frac{q_j \cdot r^3(z_1, z_j)}{D_j} \\ \frac{8}{l^2} \bar{u}_2 = \frac{q_2}{H_2} \sum_{\substack{j=1 \\ j \neq 2}}^3 \frac{C_2^3 r^3(z_2, z_j)}{D_2} + \frac{C_2}{H_2} \sum_{\substack{j=1 \\ j \neq 2}}^3 \frac{q_j \cdot r^3(z_2, z_j)}{D_j} \\ \frac{8}{l^2} \bar{u}_3 = \frac{q_3}{H_3} \sum_{\substack{j=1 \\ j \neq 3}}^3 \frac{C_3^3 r^3(z_3, z_j)}{D_3} + \frac{C_3}{H_3} \sum_{\substack{j=1 \\ j \neq 3}}^3 \frac{q_j \cdot r^3(z_3, z_j)}{D_j} \\ \frac{8}{l^2} \bar{u}_4 = \frac{C_4}{H_4} \sum_{\substack{j=1 \\ j \neq 4}}^3 \frac{q_j \cdot r^3(z_4, z_j)}{D_j} \\ \dots \\ \frac{8}{l^2} \bar{u}_n = \frac{C_n}{H_n} \sum_{\substack{j=1 \\ j \neq n}}^3 \frac{q_j \cdot r^3(z_n, z_j)}{D_j} \end{array} \right. \quad \begin{array}{l} \text{with } C_i = \frac{64 \cdot EA}{3l^2 H_i}, \\ H_i = \left( \frac{Q_i^2 \cdot l^2 EA}{24} \right)^{1/3}, \\ D_j = \sum_{k=1}^n r^3(z_k, z_j) \cdot C_k \end{array} \quad (28)$$

9 The solution vector  $\mathbf{u}$  of the above system contains the maximum displacements  
10 of the cables, i.e.  $\mathbf{u}^T = \{\bar{u}_1 \quad \bar{u}_2 \quad \bar{u}_3 \quad \bar{u}_4 \quad \dots \quad \bar{u}_n\}$  at the time instant  $t$  at which  
11 the acting loads are considered.  
12 The resulting system of non-linear differential equations (25) can be observed to  
13 be characterised by decoupled equations, since the effective coupling between the  
14 horizontal displacement is approximately accounted for by the relation given by  
15 Eq. (19a) which must be assessed from the value of the exponent  $m$ .  
16  
17 The above described mechanical model has been implemented in a simple in-  
18 house made Fortran code operating in two phases: i) determination of the  
19 function  $r(z_j, z_i)$  (defined through the exponents  $m_{ij}$ ) by the knowledge of the  
20 mechanical and geometrical characteristics of the horizontal cables and of the  
21 ‘equivalent’ vertical ones (representing the net) by using the Genetic Algorithm;  
22 ii) assessment of the displacements and forces in the deformed barrier in the time

1 domain (corresponding to the time interval of the debris impact on the structure),  
 2 by using Eqs (8, 11, 13) calculated at discrete time intervals into which the total  
 3 computation time has been subdivided. Obviously, the second phase of the  
 4 calculation requires the evaluation of the external loads acting on the barrier  
 5 (through Eqs (1-6)) throughout the entire duration of the debris flow  
 6 phenomenon.

### 8 **3.3. Modelling of the brake devices**

9 As recalled at the beginning of the paper, real barriers are usually provided by  
 10 brake system that enables to dissipate energy and to increase the cable length by  
 11 allowing a beneficial reduction of the tension in the horizontal cables.  
 12 Usually, such devices becomes effective when the maximum tensile brake force is  
 13 attained during the loading process; after that, the brake maintains such a  
 14 maximum characteristic force and dissipates energy, up to the development of the  
 15 maximum brake elongation. Once such maximum brake stroke is reached, the  
 16 device loses its function and the force in the cable starts to increase again.  
 17 The force-displacement relationship for the brake device placed on the cable  $i$  can  
 18 be written as:

$$f_b = \begin{cases} T_i \cong H_i & \text{if } T_i < f_{b,\max} \text{ and } s_b = 0 \\ f_{b,\max} & \text{if } T_i > f_{b,\max} \text{ and } s_b \leq s_{b,\max} \\ T_i \cong H_i & \text{if } s_b > s_{b,\max} \end{cases} \quad (29)$$

19 where  $f_b, f_{b,\max}, s_b, s_{b,\max}$  are the generic force, the maximum allowable brake  
 20 force, the generic displacement and the maximum brake displacement,  
 21 respectively. In order to take into account such a mechanical behaviour, the  
 22 above formulated model can be modified as follows: i) check if the force in a  
 23 generic cable reaches the maximum allowable brake force,  $f_{b,\max}$ ; ii) if the  
 24 previous condition is fulfilled (ie.  $T_i > f_{b,\max}$ ) increase the cable length by a small  
 25 fraction  $\Delta s_b$  of the original cable length in order to obtain the new effective cable  
 26 length,  $L_i = (l_i + \Delta s_b) \cdot (1 + H_i / E_i A_i)$ ; iii) determine again the force in the cable  
 27 with such a new length by using Eqs (11, 12); iv) check whether the new force is  
 28 lower than  $f_{b,\max}$  otherwise go to step ii) and increase again the cable length.

1 Repeat the above procedure until the fulfilment of the condition  $T_i < f_{b,\max}$  or  
2 continue without any other modification if the maximum brake elongation  $s_{b,\max}$   
3 has been reached.  
4 Finally, the energy dissipated by the brake during its service can be easily  
5 obtained as:

$$E_b = f_{b,\max} \cdot s_b \quad (30)$$

6

## 7 **4. Numerical applications, experimental validation** 8 **and discussion**

### 9 **4.1. Parametric numerical examples**

10 In the present section a representative example of retention barrier is considered  
11 and solved through the developed model, in order to simulate its mechanical  
12 behavior by varying some parameters of the barrier itself and of the debris flow.  
13 In particular, the effect of the stiffness of the net connecting to the horizontal  
14 cables and, for a given barrier configuration, the influence of the debris flow  
15 velocity  $v_0$  are considered.

16 The parameters of the flowing debris and those of the barrier are the following:

17  $k = 0.8, \alpha = 2.0, h_0 = 0.7m, \theta = 40^\circ, h_B = 5.0m, p = 1.0m,$

18  $f_{b,\max} = 60kN, s_{b,\max} = 0.5m$  while the transversal cables representing the net have

19 been assumed to be characterized by the ‘equivalent’ cross sectional area equal to  
20 the following values:  $A_t = 0.5mm^2, 10mm^2, 50mm^2, 200mm^2$ . In order to

21 investigate the effect of the debris flow velocity (by assuming for such a case

22  $A_t = 0.5mm^2$ ), the following values have been considered:

23  $v_0 = 2.0m/s, 4.0m/s, 8.0m/s$ . The geometry of the barrier is reported in Fig. 11a

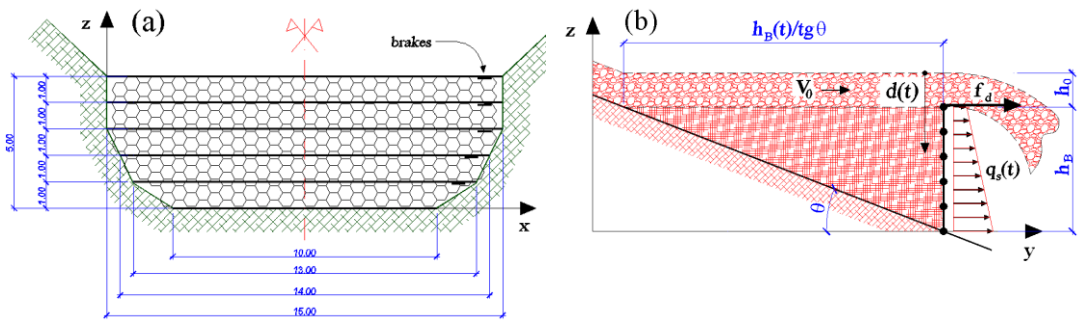
24 (the cable No 1 located at  $z = 0$  is assumed to be fixed, i.e. it does not undergo  
25 any significant displacement), while in Fig. 11b the scheme of the so-called drag

26 force  $f_d$  – occurring when the allowable volume for the debris accumulation is

27 completely filled by the flowing material – is represented when the flow continues

28 to take place above the barrier.

1



2 *Fig. 11. Geometrical dimensions of the considered barrier (a) and scheme of the*  
3 *drag force occurring when the debris flow continues above the barrier (b)*  
4 *(dimensions are expressed in m).*

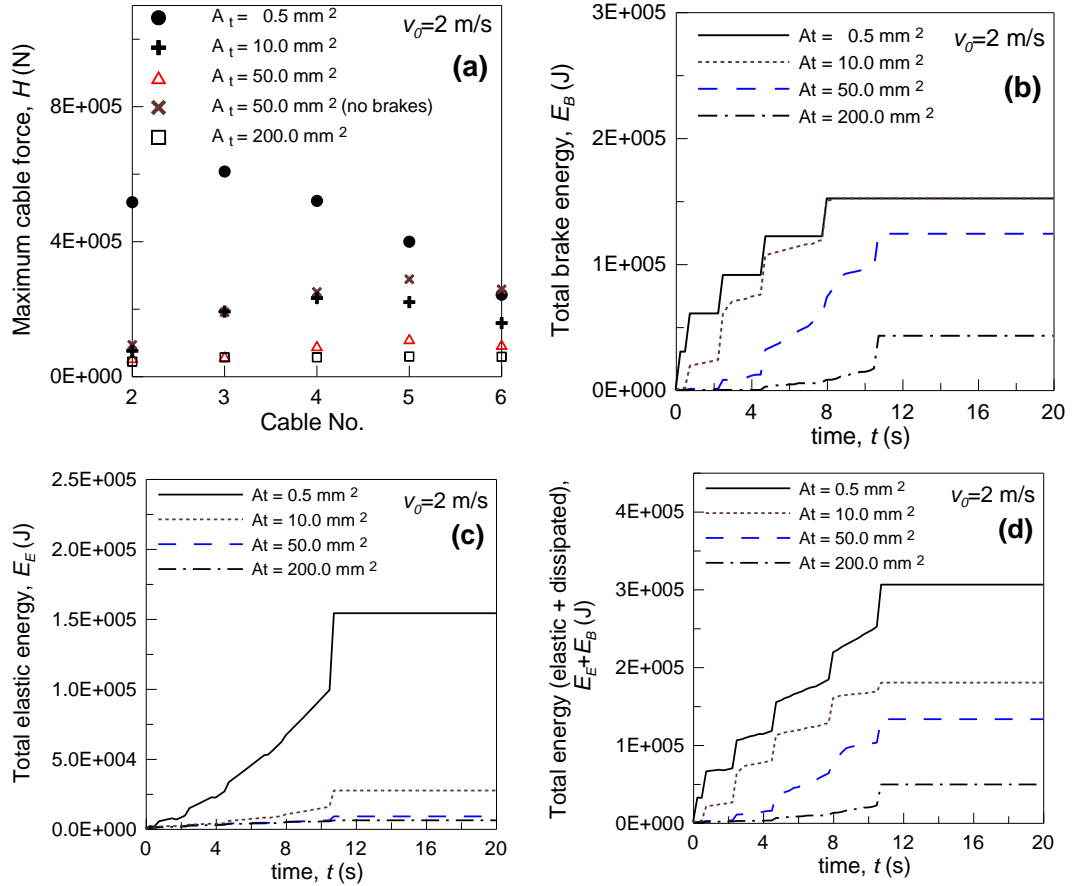
5

6 In Fig. 12 the effect of the different values of the cross section of the vertical  
7 cables is presented. In particular in Fig. 11a the maximum tensile force in the  
8 cable during the whole impact period of the debris against the barrier is presented;  
9 as can be noted the maximum tensile force reduces by increasing the stiffness of  
10 the net and such a maximum force becomes almost identical for all the cables. On  
11 the other hand, for a weak net the cables are subjected to very different maximum  
12 force values which are also higher than those calculated with strongest nets. The  
13 case of a barrier without brakes (with  $A_t = 50\text{mm}^2$ ) is also reported; the forces in  
14 the cables are obviously much higher than those obtained for the same barrier with  
15 the brakes.

16 In Fig. 12b the energy dissipated by all the brakes during the impact is  
17 represented. As it can be noticed, the total final amount of dissipated energy  
18 decreases when the net stiffness increases since the forces occurring in the cables  
19 are lower when the net is stiffer and therefore the brakes do not reach their final  
20 allowable stroke. In Fig. 12c, d the total elastic energy stored in the barrier and  
21 the sum of the total elastic and dissipated energy are represented vs time,  
22 respectively. The trend shown by the curves for different net stiffness is in  
23 accordance with the forces developing in the cables during the phenomenon. It  
24 can be also observed that, after reaching the complete filling of the barrier (see  
25 Fig. 11b), the phenomenon reaches a steady state and the above quantities remain  
26 constant with time.

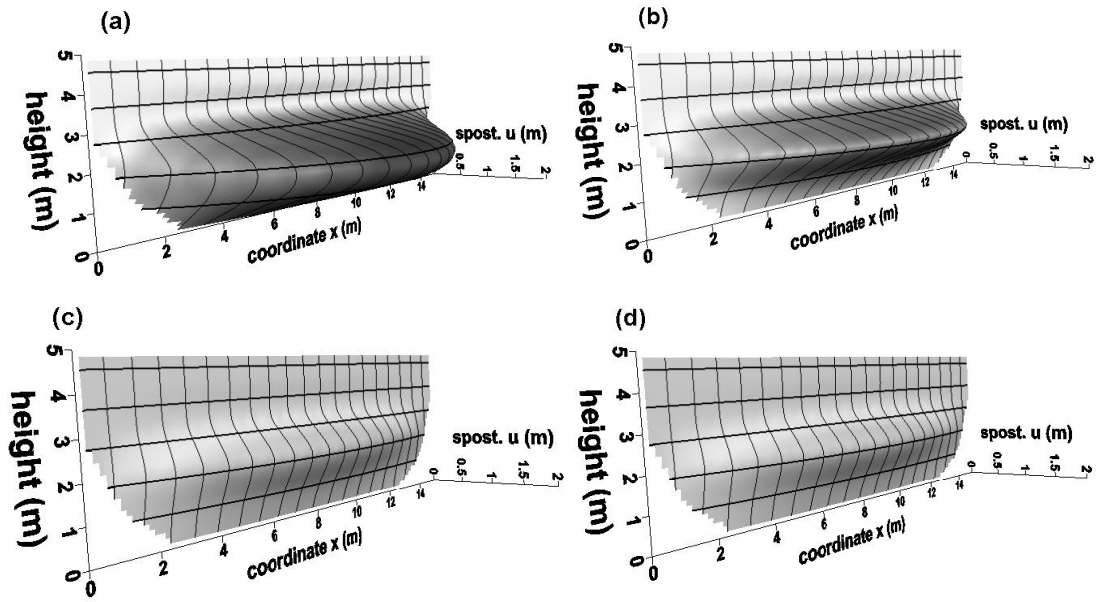


1 In Fig. 13 the deformed pattern of the barrier at the time  $t=1$ s is represented for  
 2 the four different transversal nets; it is apparent, once again, the load distribution  
 3 effect of the transversal net on the horizontal cables of the barrier.  
 4



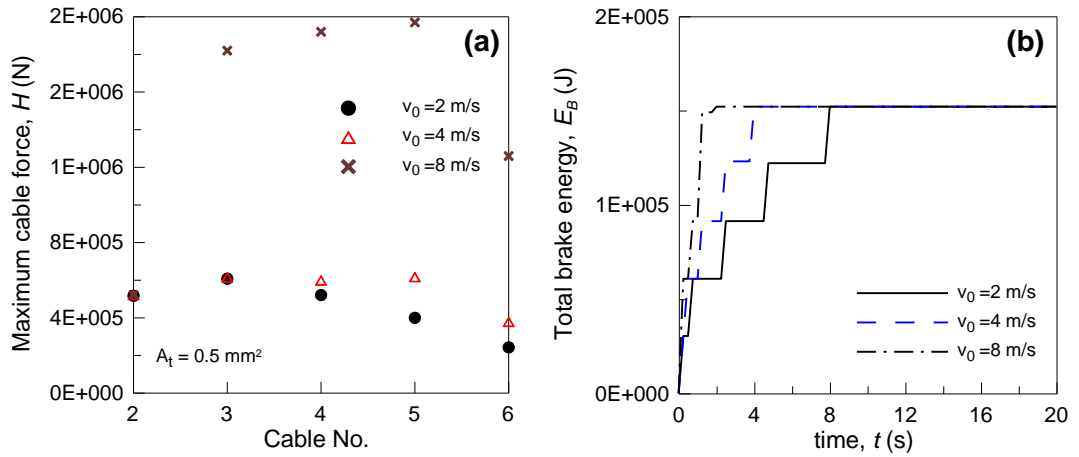
5 *Fig. 12. Barrier with different stiffness of the superposed steel net: maximum*  
 6 *tensile force in the cables (a), dissipated brake energy of the barrier (b), elastic*  
 7 *energy of the barrier (c) and total (elastic + dissipated) energy of the barrier (d)*  
 8 *vs the time  $t$ .*

9  
 10  
 11  
 12  
 13  
 14  
 15  
 16



1 Fig. 13. Deformed pattern of the barrier with different stiffness of the superposed  
 2 steel net at the time  $t=1s$ : case of  $A_t = 0.5mm^2$  (a),  $A_t = 10mm^2$  (b),  $A_t = 50mm^2$   
 3 (c) and  $A_t = 200mm^2$  (d).

4  
 5 Finally the effect of the debris flow surges velocity is herein considered. In Fig.  
 6 14 the maximum tensile force attained in the different cables of the barrier is  
 7 represented for the three assumed debris flow surges velocity  
 8 ( $v_0 = 2.0m/s, 4.0m/s, 8.0m/s$ ). It appears as the force in the bottom cable (No.  
 9 2) is not influenced by  $v_0$  since the static load produced by the accumulated  
 10 material prevails over the dynamic force; on the other hand, the velocity influence  
 11 becomes relevant for the cables placed at higher levels. In Fig. 14b the total  
 12 amount of dissipated energy is represented; it appears that such total energy at the  
 13 end of the phenomenon is the same for the different velocities since all the brakes  
 14 reach their maximum allowable sliding length. In the case of higher velocities of  
 15 the flow surges, the maximum brakes displacement is reached in a shorter time  
 16 with respect to lower velocities.  
 17



1 *Fig. 14. Effect of the debris flow velocity. Maximum tensile forces in the cable*  
 2 *during the debris impact (a) and total energy dissipated by the brakes vs the time  $t$*   
 3 *(b) for different values of  $v_0$ .*

#### 6 **4.2. Simulation of a full scale test of a retention barrier**

7 In order to assess the reliability of the proposed analytical model, the simulation  
 8 of a full scale test on a barrier is considered hereafter.

9 The test was carried out inside a limestone quarry located in the Pieve d'Alpago  
 10 district (Belluno province, Northeastern Italian Alps); the artificial channel was  
 11 built by re-shaping an existing natural impluvium and the barrier was located at its  
 12 bottom (Fig. 4). The obtained artificial channel was 2 m large and 48 m long, with  
 13 an average slope of  $40^\circ$ . The material used to simulate the flow was constituted by  
 14 well-graded limestone blocks with diameter ranging from few cm to 1.5 m. Due to  
 15 the particular geometry of the channel, to the nature of the material and to the  
 16 machinery used to mobilize it, it was not possible to keep the material saturated;  
 17 however, the effects on the barrier in terms of deformation and forces were in  
 18 good agreement with other small scale and large scale test results available in  
 19 bibliography (Davies [52], Iverson [53], Canelli [41]).

20 During the test, both deformation and horizontal cable forces were measured  
 21 using photogrammetric techniques and load cells, respectively. The  
 22 photogrammetric restitution was based on the pictures taken by a couple of frontal  
 23 high definition camera that shot at a speed of 23 frame per second. The load cells,  
 24 with a maximum measurement range of 1000 kN, were mounted on each of the

1 five horizontal cables as depicted in Figure 2 and their data were recorded at 1 Hz  
2 frequency.

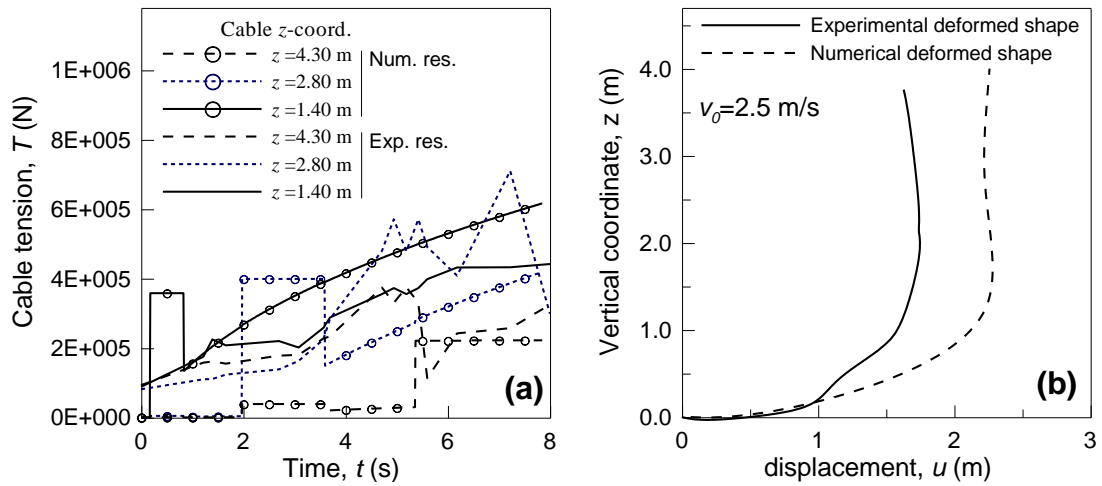
3 The registered flow velocity was 2.51 m/s on average with measured peaks of 9  
4 m/s, the total volume stopped at the barrier was of approximately 400 m<sup>3</sup>, the  
5 average flow height  $h_0$  was equal to 0.7 m while the material density was  
6 estimated in 1790 kg/m<sup>3</sup>. The test came to the end with the filling up of the whole  
7 barrier, no overflow was allowed in order to preserve the safety at test site.

8 The structure under consideration is characterized by an average span of about  
9 17.00 m while its height is equal to 4.00 m; it is composed by four main  
10 horizontal double steel cables (6x19 class according to UNI EN 12385-4) having  
11 diameter  $\phi 20$  mm, fixed at the extremities to foundations grouted inside the  
12 channel shoulders. The four horizontal main cables are mounted at a relative  
13 vertical distance  $p$  equal to about 1.33 m (Fig. 2). A steel ASM 3-4- 350/200 ring  
14 net made by  $\phi 350$  mm rings, connected at four point contact is linked at the  
15 horizontal cables (Fig. 3). The rings are formed by a single steel wire (1380  
16 N/mm<sup>2</sup> minimum tensile strength) having a diameter  $\phi 3$  mm and rolled up in 10  
17 loops and 2 spirals. The lower cable was fixed at the bottom surface of the  
18 channel in the real test, by means of several anchors; in order to account for the  
19 effect of those restrains in the analytical model, since the proposed simplified  
20 analytical model does not allow the application of restraint along the main cables,  
21 a cable with a larger cross sectional area (20 times the area of the others) was  
22 adopted. This assumption implies that the horizontal displacements of the lower  
23 cable are negligible and its calculated axial forces are omitted for the comparison  
24 between real case and numerical results.

25 The analytical model has been solved by assuming  $\alpha = 1.5$ ,  $k = 0.5$  to describe  
26 the loads on the barrier; the value of the empirical coefficient  $\alpha$  and of the earth  
27 pressure coefficient  $k$  were recovered through back analysis, considering the  
28 indications of Canelli et al. [41] and Bugnion et al. [54] while the exponent  $m$  of  
29 the functions  $r(z_j, z_i)$  relating each cable with the others - i.e. for the assessment  
30 of the cables interaction - have been calculated according to the above described  
31 GA procedure.

32 The values of the coefficients necessary for the evaluation of the forces induced  
33 by the debris flow against the barrier (Eqs 1, 3), have been performed by  
34 following the considerations below.

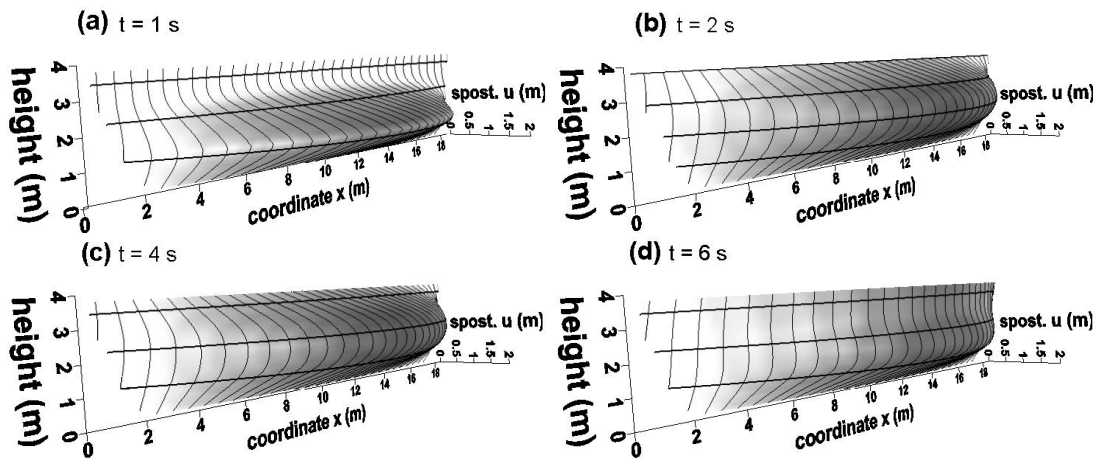
1 Bugnion et al. [54] have performed several tests of flow against obstacles and  
 2 computes the  $\alpha$  value. They shows that 2 is the maximum value. For this reason  
 3 the Authors considered this value in the initial phase of development of the work.  
 4 For the coefficient of earth pressure  $k$ , the value  $k = 0.5$  was chosen because Kwan  
 5 and Cheung [40] suggested a maximum value of 1 in undrained condition but we  
 6 could observe a condition of partial saturation during the flow and of good  
 7 drainage during the impact of the debris against the barrier. Therefore, the friction  
 8 angle of the debris accumulation behind the barrier was originally assumed  
 9 between  $20^\circ$  and  $30^\circ$ , converging to the value of  $20^\circ$  through a back analysis  
 10 procedure developed in order to better fit the experimental results.  
 11



12 *Fig. 15. Comparison between experimental and analytical results of: (a) tension*  
 13 *forces in the horizontal structural cables vs. time; (b) maximum deformed shape*  
 14 *of the barrier at the midspan vertical section.*

15  
 16 In Fig.15 (a) the forces measured in each cable (identified through its co-ordinate  
 17 position  $z$ ) during the test are plotted against time, together with those determined  
 18 using the proposed analytical model. In Fig. 15 (b) are reported both the shape of  
 19 the deformed barrier measured at the central vertical section at the end of the test  
 20 and that calculated using the proposed model. Although some differences  
 21 between experimental and numerical results were obtained, especially for what it  
 22 concerns the barrier deformation, the induced state of traction in the cables are in  
 23 good agreement. This is possibly due to the initial state of stress in the cables,  
 24 which is originally applied during the structure assembly; this pretension is not  
 25 influencing the final state of stress induced by the debris flow impact while it

1 does, instead, influence its deformation particularly at the beginning and at the  
 2 end of the loading process. Furthermore, the lower portion of the barrier (lower  
 3 horizontal cable) is free to deform along its length in the proposed model (its  
 4 displacement is fictitiously limited by adopting a cable cross section area greater  
 5 than its effective value, as already discussed) while, in the real case, is fixed at the  
 6 channel surface by means of eyebolts. These boundary conditions can be  
 7 reconsidered and improved in future development of the work.  
 8 Regarding the duration of the test reported in abscissa in Fig. 15 (a), it should be  
 9 considered that, while in the analytical model it is calculated using the geometry  
 10 of the channel and the velocity of the debris surge, for what it concerns the real  
 11 test it is determined considering the debris flow as if it was flowing at a constant  
 12 rate, neglecting the interruptions that occurred between surges due to the above  
 13 described operational limitations.  
 14



15 *Fig. 16. Deformed patters provided by the present model for  $t=1.0$  s (a),  $t=2.0$  s*  
 16 *(b),  $t=4.0$  s (c) and  $t=6.0$  s (d) (see Fig. 15b) corresponding to the simulation of*  
 17 *the on site tests described above.*

18  
 19 In Fig. 16 a full 3-dimensional reconstruction of the net deformed pattern during  
 20 the loading process is also given; as can be observed it shows how the method can  
 21 realistically reproduce the barrier deformation with the time, providing the net  
 22 shape as the flow phenomena proceeds and the debris accumulates behind the  
 23 retention barrier. This results can be usefully applied in the future for setting up a  
 24 real time net monitoring system able to define threshold values to be controlled in  
 25 situ by means of specific measuring devices.

1 The energy dissipated by the barrier upon the impact with the debris flow can be  
 2 calculated by adding two terms: the first derived from the dissipation of the brake  
 3 devices  $E_b$  and the second induced by the elastic deformation of the supporting  
 4 cables  $E_E$  (see Eq. (31)).

$$\begin{aligned} E_b &= f_{b,\max} \cdot s_b, \\ E_E &= 1/2(LH^2 / EA) \end{aligned} \quad (31)$$

5 In our simulation of the test, the amount of energy dissipated at the end of the  
 6 impact phase is approximately equal to 286 kJ.  
 7 Sun & Law [55] proposed several analytical solution for the determination of the  
 8 design impact energy of the barrier based upon pile-up or run-up mechanisms. In  
 9 our case, the most appropriate formulation appears to be the run-up mechanism  
 10 with the height of the final debris accumulation equal to the height of the barrier.  
 11 The related equation, proposed by Sun & Law [55] and rewritten with our  
 12 notations becomes:

$$E_B = \frac{\rho_d Fr v_0 h_b^2}{4h_0 \tan(\theta + \alpha)} - \frac{\rho_d g Fr h_b^3}{3h_0 v_0 \tan(\theta + \alpha) \sin(\theta + \alpha)} (\sin \alpha + \mu \cos \alpha) \quad (32)$$

13 The application of Eq. (32) to the Pieve d'Alpago test, considering the parameters  
 14 acquired from the back analysis described above, gives a design impact energy of  
 15 the barrier  $E_B$  equal to 452 KJ. This result is obtained considering the angle  
 16 between the horizontal and the upper surface of the debris accumulated behind the  
 17 barrier substantially horizontal ( $\alpha = 1^\circ$ ) as observed during the test. The interface  
 18 friction coefficient  $\mu$  is determined, using Eq. (33) described in [55] through a  
 19 back analysis procedure aimed at obtaining the impact duration  $T_f$  comparable  
 20 with that calculated by the proposed analytical model (approximately 8 s).  
 21

$$T_f = \frac{h_b^2}{2v_0 h_0 \tan(\theta + \alpha)} \quad (33)$$

22 The above consideration indicates that around 37% of the design impact energy  
 23 of the debris flow is dissipated internally during the impact phase and only the  
 24 remaining portion is transferred to the barrier.

## 1 **5. Conclusions**

2 The energy associated with debris flows along with their velocity, active volumes  
3 and run out distances have often made these phenomena very destructive and  
4 dangerous. The design of retention devices, which are often a must in populated  
5 area or wherever it is necessary to limit the destructive effects of debris flows, is  
6 often carried out using previous experiences and subjective knowledge of the  
7 phenomena mechanics. Analytical approaches are seldom used and generally  
8 based on numerical modelling (FEM). However, the numerical modelling of  
9 these structures, which should be carried out considering the debris flow impact  
10 dynamics, can turn out to be very complicated and not always reliable in  
11 applicative cases. For these reasons, the need of a sound design instrument, easily  
12 applicable in standard, is becoming of paramount importance and is not yet  
13 available to practitioners.

14 In the present paper a simplified analysis of the mechanics of debris-flow is  
15 considered in order to estimate the forces developed by such a flow impacting on  
16 a retention barrier. Then, an analytical simplified structural model of cable-like  
17 retention barriers is developed, based on the equation of equilibrium of wires  
18 under large displacements condition, and the restraining forces as well as the  
19 cable stresses are finally estimated. A parametric study has been presented, in  
20 order to demonstrate the capability of the proposed model to capture all the main  
21 mechanical aspect occurring during the impact of a debris flow against a flexible  
22 structure. The boundary conditions for the lower cable are the same as those listed  
23 for the other cables (i.e. anchored at the channel sides), avoiding to consider the  
24 lower cable connected to the channel bottom. This geometrical configuration is  
25 often used, in consideration of the scarce mechanical reliability of the debris  
26 deposited along the channel.

27 The comparison between experimental and numerical results has been presented,  
28 as well. The satisfactory agreement hereby shown, enable us to state that the  
29 present approach is promising, even though, some differences have been recorded;  
30 such discrepancies are possibly due to the simplifying variables introduced in the  
31 calculation and to some of the theoretical assumption needed to achieve an  
32 analytical solution of the problem. However, this work represents a starting point  
33 that will need further development along with additional validations. At present,  
34 new experimental data are processed (either taken from literature or from direct



1 measurements) and several parametric analysis are under development in order to  
2 define the sensitivity of the model upon changes in the structural geometry or in  
3 the debris flow features.

4

## 5 **Acknowledgements**

6 The authors gratefully acknowledge the research support for this work provided by the Italian  
7 Ministry for University and Technological and Scientific Research (MIUR) and by the ICE  
8 (Institute for Foreign Commerce). We also wish to acknowledge the financial and technical  
9 support of Consorzio Triveneto Rocciatori S.C.r.l. and Officine Macaferri S.p.a. (Italy).

10

11

## 12 **References**

- 13 [1] Takahashi T (1983) Debris flow and debris flow deposition. In: *Advances in the Mechanics*  
14 *and Flow of Granular Materials*, Vol. II. Shahinpoor M. (ed.) Trans. Tech. Publ. 57–77.
- 15 [2] Govi M, Mortara G, Sorzana PF (1985) Eventi Idrogeologici e Frane, *Geologia Applicata e*  
16 *Idrogeologia*, Vol. XX, Part II, 359–375.
- 17 [3] Pierson TC, Costa JE (1987) A rheologic classification of subaerial sediment-water flow. *Geol.*  
18 *Soc. Am., Rev. Eng. Geol.* 7: 112.
- 19 [4] Costa JE (1984) Physical geomorphology of debris flows. In J.E. Costa & P.J. Fleisher (eds),  
20 *Developments and Applications of Geomorphology*. New York, Springer-Verlag: 268–317.
- 21 [5] Phillips CJ, Davies TRH (1991) Determining rheological properties of debris flow material.  
22 *Geomorphology* 4: 101–110.
- 23 [6] Meunier M (1991) *Eléments d'hydraulique torrentielle*. CEMAGREF Etudes, Série Montagne,  
24 n. 1: 278.
- 25 [7] Wan Z, Wang Z (1994) *Hyperconcentrated Flows*, IAHR Monograph Series, Balkema,  
26 Rotterdam.
- 27 [8] Coussot P., Meunier M. (1996) Recognition, classification and mechanical description of  
28 debris flows. *Earth-Science Reviews* 40: 209–227.
- 29 [9] Hungr O, Evans SG, Bovis MJ, Hutchinson JN (2001) A review of the classification of  
30 landslides of the flow type. *Environmental and Engineering Geoscience* 7(3): 221–238.
- 31 [10] Takahashi T (2007) *Debris flow. Mechanics, Prediction and Countermeasures*. Taylor and  
32 Francis/Balkema: 33-157 & 211-254
- 33 [11] Okuda S, Suwa H, Okunishi K, Yokoyama K, Nakano M (1980) Observations on the motion  
34 of a debris flow and its geomorphological effects. *Zeitschrift für Geomorphologie N.F.*,  
35 *Suppl. Bd.*, 35: 142–163.
- 36 [12] Marchi L, Arattano M, Deganutti M (2002) Ten years of debris-flow monitoring in the  
37 Moscardo Torrent (Italian Alps). *Geomorphology* 46 (1/2): 1–17.
- 38 [13] Hürlimann M, Rickenmann D, Graf C (2003) Field and monitoring data of debris-flow events  
39 in the Swiss Alps. *Canadian Geotechnical Journal* 40 (1): 161–175.

- 1 [14] Tecca PR, Deganutti AM, Genevois R, Galgaro A (2003) Velocity distribution in a coarse  
2 debris flow. In Debris-flow hazard mitigation: Mechanics, Prediction and Assessment. Proc.  
3 of the 3rd Int. DFHM Conference. Davos, CH. Sept. 10-12, 2003. D. Rickenmann & C.L.  
4 Chen (eds). Rotterdam, Millpress: 905–916.
- 5 [15] Iverson RM (1997) The physics of debris flows. *Review of Geophysics* 35, 3:45–296.
- 6 [16] Mizuyama T, Uehara S (1983) Experimental study of the depositional process of debris flow.  
7 *Japanese Geomorphological Union* 4 (1): 49–63.
- 8 [17] Liu GR, Lee FC, Tsai HP (1997) The flow and impact force on a debris dam. *Debris-flow*  
9 *Hazards Mitigation*, ASCE, New York: 737–746.
- 10 [18] Chau KT, Chan LCP, Luk ST, Wai WH (2000) Shape of deposition fan and runout distance  
11 of debris-flow: effects of granular and water contents. In “Debris-Flow Hazards Mitigation:  
12 Mechanics, Prediction and Assessment”. Rotterdam, Wieczorek & Naeser (eds) Balkema:  
13 387–395.
- 14 [19] Deganutti AM, Tecca PR, Genevois R, Galgaro A (2003) Field and laboratory study on the  
15 deposition features of a debris flow. In D. Rickenmann & C.L. Chen (eds), *Debris-flow*  
16 *Hazards Mitigation: Mechanics, Prediction, and Assessment; Proceedings of the 3rd*  
17 *International DFHM Conference. Davos, Switzerland, Sempt. 10-12, 2003. Rotterdam,*  
18 *Millpress: 833–841.*
- 19 [20] Ghilardi P, Pagliardi M, Zanittigh B (2006) Analisi sperimentale del processo di impatto di  
20 miscele granulari sature contro pareti verticali. XXX Convegno di Idraulica e Costruzioni  
21 Idrauliche, IDRA 2006.
- 22 [21] Major J. J. (1997) Depositional Processes in Large Scale Debris Flow Experiments. *The*  
23 *Journal of Geology*. Vol. 105, No. 3, May 1997, pp. 345-366
- 24 [22] Ferrero A M, Giani G P, Segalini A (2010) Numerical and experimental analysis of debris  
25 flow protection fence efficiency. *Proc. European Rock Mechanics Symposium (Eurock*  
26 *2010), Lausanne, CH. Balkema, Rotterdam: 578-578*
- 27 [23] Olivares L, Picarelli L (2001) Susceptibility of loose pyroclastic soils to static liquefaction:  
28 some preliminary data, in: *Proc. Of Int. Conf. on Landslides – Causes, Impacts and*  
29 *Countermeasures, Davos, 75–85.*
- 30 [24] Hungr O, Evans SG (1996) Rock avalanche runout prediction using a dynamic model. In:  
31 Senneset, K. (Ed.), *Proc. of the 7th International Symposium on Landslides, Trondheim.*  
32 *A.A. Balkema, Rotterdam, 233–238.*
- 33 [25] Pirulli M (2005) Numerical modelling of landslide runout, a continuum mechanics approach.  
34 PhD Thesis, Department of Structural and Geotechnical Engineering, Politecnico di Torino,  
35 Italy.
- 36 [26] Vallance JW (1994) Experimental and field studies related to the behaviour granular mass  
37 flows and the characteristics of their deposits. Ph.D. thesis, Michigan Technological  
38 University.
- 39 [27] Cesca (2008) Debris-flow runout predictions based on the average channel slope  
40 (ACS) *Original Research Article Engineering Geology, Volume 98, Issues 1–2, 21 April*  
41 *2008, 29–40.*

- 1 [28] Bagnold RA (1954) Experiments on a gravity-free dispersion of large solid spheres in a  
2 Newtonian fluid under shear Proc. R. Soc. Lond. A, 225: 49–63.
- 3 [29] Goldhirsch I (2003) Rapid Granular Flows, Annual Review of Fluid Mechanics 35: 267–293.
- 4 [30] Jenkins JT, Hanes DM (1998) Collisional sheet-flow of sediment driven by a turbulent fluid.  
5 J. Fluid Mech. 370: 29–52.
- 6 [31] Hanes DM, (1998) Collisional sheet flows of sediment driven by a turbulent fluid. Fluid  
7 Mechanics 370: 29–52.
- 8 [32] Armanini A, Fraccarollo L, Larcher M (2008) Liquid-granular channel flow dynamics.  
9 Powder Technology 18, 2: 218–227.
- 10 [33] Chen H, Lee CF (2000) Numerical simulation of debris flows. Canadian Geotechnical Journal  
11 37, 1: 146.
- 12 [34] Denlinger RP, Iverson RM (2004) Granular avalanches across irregular three-dimensional  
13 terrain: 1. Theory and computation.3 J. of Geophysical Res. 109: F01014: 14.
- 14 [35] McDougall S, Hungr O (2004) A model for the analysis of rapid landslide motion across  
15 three-dimensional terrain. Canadian Geotechnical Journal 41, 1084–1097.
- 16 [36] Savage SB, Hutter K (1989) The motion of a finite mass of granular material down a rough  
17 incline. J. of Fluid Mechanics 199: 177–215.
- 18 [37] Suwa H, Okuda S (1983) Deposition of debris flows on a fan surface, Mt. Yakedake, Japan.  
19 Z. Geomorphol. Suppl. 46: 79–101.
- 20 [38] Hungr O (1985) A model for the runout analysis of rapid flow slides, debris flows, and  
21 avalanches. Can Geotech J. 32: 610–623.
- 22 [39] Van Dine DF (1996) Debris Flow Control Structures for Forest Engineering. Province of  
23 British Columbia Ministry of Forests Research Program, 68.
- 24 [40] Kwan J.S.H. & Cheung R.W.M. (2012) Suggestion on Design Approaches for Flexible  
25 Debris-resisting Barriers . Standard and Testing Division. Discussion Note DN1/2012. The  
26 Government of Hong Kong Special Administrative Region.
- 27 [41] Canelli L., Ferrero A.M., Migliazza M., Segalini A. (2012) Debris flow risk mitigation by the  
28 means of rigid and flexible barriers – experimental tests and impact analysis. Nat. Hazards  
29 Earth Syst. Sci., 12, 1–7 (www.nat-hazards-earth-syst-sci.net/12/1/2012/ doi:10.5194/nhess-  
30 12-1-2012).
- 31 [42] WSL (2009) Full-scale Testing and Dimensioning of Flexible Debris Flow Barriers. Swiss  
32 Federal Institute for Forest, Snow and Landscape Researc (WSL), 22 p.
- 33 [43] Lo D.O.K. (2000) Review of natural terrain landslide debris-resisting barrier design.  
34 Geotechnical Engineering Office Report No. 104. The Government of Hong Kong Special  
35 Administrative Region: 14–32.Major JJ (1997) Depositional processes in large-scale debris-  
36 flow experiments. The Journal of Geology 105: 345–366.
- 37 [44] Seidel M. (2009) [Tensile Surface Structures: A Practical Guide to Cable and Membrane  
38 Construction, Wiley.](#)
- 39 [45] Levy R, Spillers WR (2004) Analysis of Geometrically Nonlinear Structures, Kluwer  
40 Academic Publishers, 2nd ed.: 151–186

- 1 [46] Goldberg DE (1989) Genetic algorithms in search, optimization, and machine learning. MA,  
2 Addison-Wesley Publishing Company inc: 1-56.
- 3 [47] Gen M, Cheng R (1996) Genetic algorithms and engineering design. New York, John Wiley  
4 and Sons:1:40
- 5 [48] Gantovnik VB, Anderson-Cook CM, Gürdal Z, Watson LT (2003) A genetic algorithm with  
6 memory for mixed discrete-continuous design optimization. *Comp. & Struct.* 81: 2003–2009.
- 7 [49] Brighenti R (2005) Fibres distribution content optimisation in fibre-reinforced composite by a  
8 genetic algorithm. *Int. J. Composite Structures* 71(1): 1–15.
- 9 [50] Brighenti R, Carpinteri A, Vantadori S (2006) A genetic algorithm applied to optimisation of  
10 patch repairs for cracked plates. *Comp. Meth. App. Mech. and Engng.* 196: 466–475.
- 11 [51] Zohdi TI (2003) Constrained inverse formulations in random material design, *Comp. Meth.*  
12 *Appl. Mech. Engng* 192: 3179–3194.
- 13 [52] Davies T.R.H. (1988) Debris flow surges – a laboratory investigation. Mitteilung Nr. 96,  
14 VAW, ETH-Zurich, Switzerland.
- 15 [53] Iverson, R. M., J. E. Costa, and R. G. LaHusen (1992), Debris-flow flume at H. J. Andrews  
16 Experimental Forest, Oregon, U.S. Geol. Surv. Open File Rep., 92-483, 2 pp. (Available at  
17 [http://vulcan.wr.usgs.gov/Projects/MassMovement/Publications/OFR92-](http://vulcan.wr.usgs.gov/Projects/MassMovement/Publications/OFR92-483/framework.html)  
18 [483/framework.html](http://vulcan.wr.usgs.gov/Projects/MassMovement/Publications/OFR92-483/framework.html))
- 19 [54] Bugnion L, McArdell B.C., Bartelt P, Wendeler C. (2012) Measurements of hillslope debris  
20 flow impact pressure on obstacles. *Landslides.* 9:179-187. DOI 10.1007/s10346-011-0294-4
- 21 [55] Sun H.W. & Law R.P.H (2012) A preliminary study on impact of landslide debris on flexible  
22 barriers. Geotechnical Engineering Office. Standard and Testing Divison. Technical Note  
23 1/2012. The Government of Hong Kong Special Administrative Region.